Fluid Dynamic Structures in the Right Ventricle with Presence of Pulmonary Regurgitation after Tetralogy of Fallot Repair

Amanda Mikhail

A Thesis
In the Department
of
Mechanical, Industrial and Aerospace Engineering

Presented in Partial Fulfillment of the Requirements
For the Degree of
Master of Applied Science (Mechanical Engineering) at
Concordia University
Montreal, Quebec, Canada

November 2019

© Amanda Mikhail, 2019

CONCORDIA UNIVERSITY
School of Graduate Studies

This is to certify that the thesis prepared

By: Amanda Mikhail

Entitled: Fluid Dynamic Structures in the Right Ventricle with Presence of Pulmonary Regurgitation after Tetralogy of Fallot Repair

and submitted in partial fulfillment of the requirements for the degree of

Master of Applied Science (Mechanical Engineering)

complies with the regulations of the University and meets the accepted standards with respect to originality and quality.

Signed by the final Examining Committee:

_____ **Chair**
Dr. Hoi Dick Ng

_____ **Examiner**
Dr. Hany Gomaa

_____ **Examiner**
Dr. Sana Jahanshahi Anbuhi

_____ **Supervisor**
Dr. Lyes Kadem

Approved by _____
***Dr. Ahmed Waizuddin*, Graduate Program Director**

November 22, 2019

_____
***Dr. Amir Asif*, Dean**
Gina Cody School of Engineering and Computer Science

Abstract

Fluid Dynamic Structures in the Right Ventricle with Presence of Pulmonary Regurgitation after Tetralogy of Fallot Repair

Amanda Mikhail

Tetralogy of Fallot (TOF), which causes 8-10% of all congenital defects, is a concern for 1 in 2518 parents. Although the effects of this disease can be remedied by a surgery at birth, regurgitation from the pulmonary valve seems to occur two to three decades after this repair in 50% of the operated cases. Since little is known regarding the cause of this regurgitation or simply the natural flows in the right ventricle (RV), this research, which is the first of its kind, aims to shed light on fluid flow in the right ventricle during normal function as well as the effects on the fluid flow due to the introduction of regurgitation from the pulmonary valve. An in-house cardiovascular simulator was used to simulate the pumping action of the right ventricle through the use of a linear motor, which gave rise to the E-wave, while a servo motor gave rise to the A-wave. Various severities of regurgitation, defined by ratio of the effective regurgitant orifice area over the total valve orifice area (ROA/A), (0 ROA/A, 0.012 ROA/A, 0.063 ROA/A and 0.174 ROA/A) were simulated through the restriction of the valve closure while the fluid used was a 60%-40% water-glycerol mixture in order to mimic human blood viscosity. Planar time-resolved particle image velocimetry measurements have been performed on a custom-made double activation simulator reproducing flow conditions in a model of a right ventricle. Changes in flow characteristics in the right ventricle have been evaluated in terms of velocity fields and profiles, tricuspid inflow jet orientation and viscous energy dissipation. Our results show that pulmonary valve regurgitation significantly alters the flow in the right ventricle mostly by impairing the

diastolic inflow through the tricuspid valve and by increasing viscous energy loss. This fundamental work should allow for a better understanding of such changes in the RV flow dynamics. It may also help in developing new strategies allowing for a better follow-up of patients with repaired TOF and for decision-making in terms of pulmonary valve replacement.

Acknowledgements

I want to first and foremost thank God for giving me the faith and strength to hang in there when times were challenging and for helping me persevere in my research. Secondly, I want to thank my parents, who have always encouraged me and told me that I could achieve anything I set my mind to. They have supported me from the very beginning and I know they will always root for me in all of my future endeavours.

A big thank you to Dr Lyes Kadem for giving me the opportunity to work in his lab and for giving me this project. Truth is, he has done so much more; he gave me the chance to attend conferences, which has allowed me to expand my knowledge regarding our field and to gain a taste for the "outside world". He has created such a supportive environment in his lab that it has been a pleasant and enjoyable experience to be there and has been a great support to me during the times when I would question my abilities. Overall, a big thank you is owed.

I also want to thank all of my colleagues in the lab which have humoured me and listened to my obstacles regarding my research and have helped me to the best of their abilities. On this point, I want to give a special thank you to Giuseppe Di Labbio who has taken the time since I've arrived at the lab to explain to me everything, always took the time to answer my questions throughout my time in the lab, and has become a good friend.

As mentioned previously, I want to thank all of my colleagues that have not only given me help throughout my work but have also given me friendships and memories to cherish: Shahrzad Norouzi, Maziar Sargodi, Ahmed Darwish, Ghazaale Zeinaly, Nasibeh Mirvakili, Yusri Al-Sanaani and Max Lavigne.

Lastly, I want to say how this research has not only allowed me to increase my knowledge academically but has given me so much more; amazing colleagues and friends, plenty of new experiences and the opportunity to grow on a personal level.

Table of Contents

Table of Figures

List of Tables

List of Symbols

Latin

A	Area (m^2)
A_r	Constant of extrapolation
A_k	Constant of extrapolation
C	Covariance matrix
G	Eigenvector matrix
H	Global entropy
h value	Statistical difference
L	Ventricle length (m)
N	Total number of modes
n	Angular frequency (1/s)
p	Energy fraction of a mode
p value	Statistical significance
PIV	Particle image velocimetry
POD	Proper orthogonal decomposition
R	Radius (m)
ROA	Regurgitant orifice area (m^2)
T	Time (s)
t*	Diastolic time (s)
u	Velocity component in the x direction (m/s)
U	Velocity matrix
V	Velocity (m/s)
V_{max}	Maximum velocity (m/s)
v	Velocity component in the y direction (m/s)
VED	Viscous energy dissipation (W/m)
Wo	Womersley number
x	Particle position (m)

Greek

Γ	Circulation (m^2/s)
Δt	Duration between laser pulses (μs)
λ	eigenvalue matrix
μ	Dynamic viscosity (Pa·s)
ρ	Density (kg/m^3)
ϕ	Spatial mode
ψ	Spatial mode matrix
ω	Vorticity (1/s)

Chapter 1 - Background

1.1 The Cardiovascular System

The functioning of the human body is critically dependent on the proper functioning of the heart. Since it is the leading cause of death in both Canada and the United States [1], it comes as no surprise that there is currently extensive research in the field of cardiac diseases and congenital defects. To better comprehend the purpose of this thesis, an understanding of the functioning of a normal heart is necessary. The normal blood flow through a heart is depicted in Figure 1.

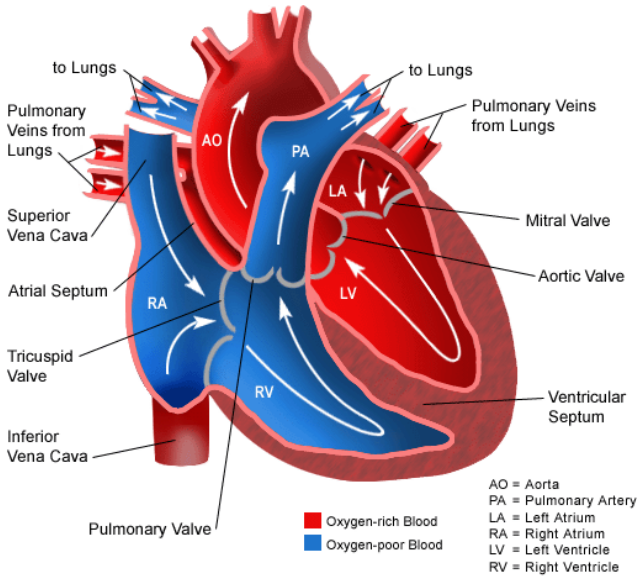

Figure 1.1: Blood flow through a normal heart [2]

The flow through the human body is a closed circuit comprised of three main subsystems; the systemic circuit which is the blood flow supplied by the aorta and feeds the whole body, the pulmonary system which is supplied by the pulmonary artery and oxygenates blood at the lungs,

and the coronary system which is, in essence, the blood supply for the heart. Figures 2 and 3 show the layout of these subsystems.

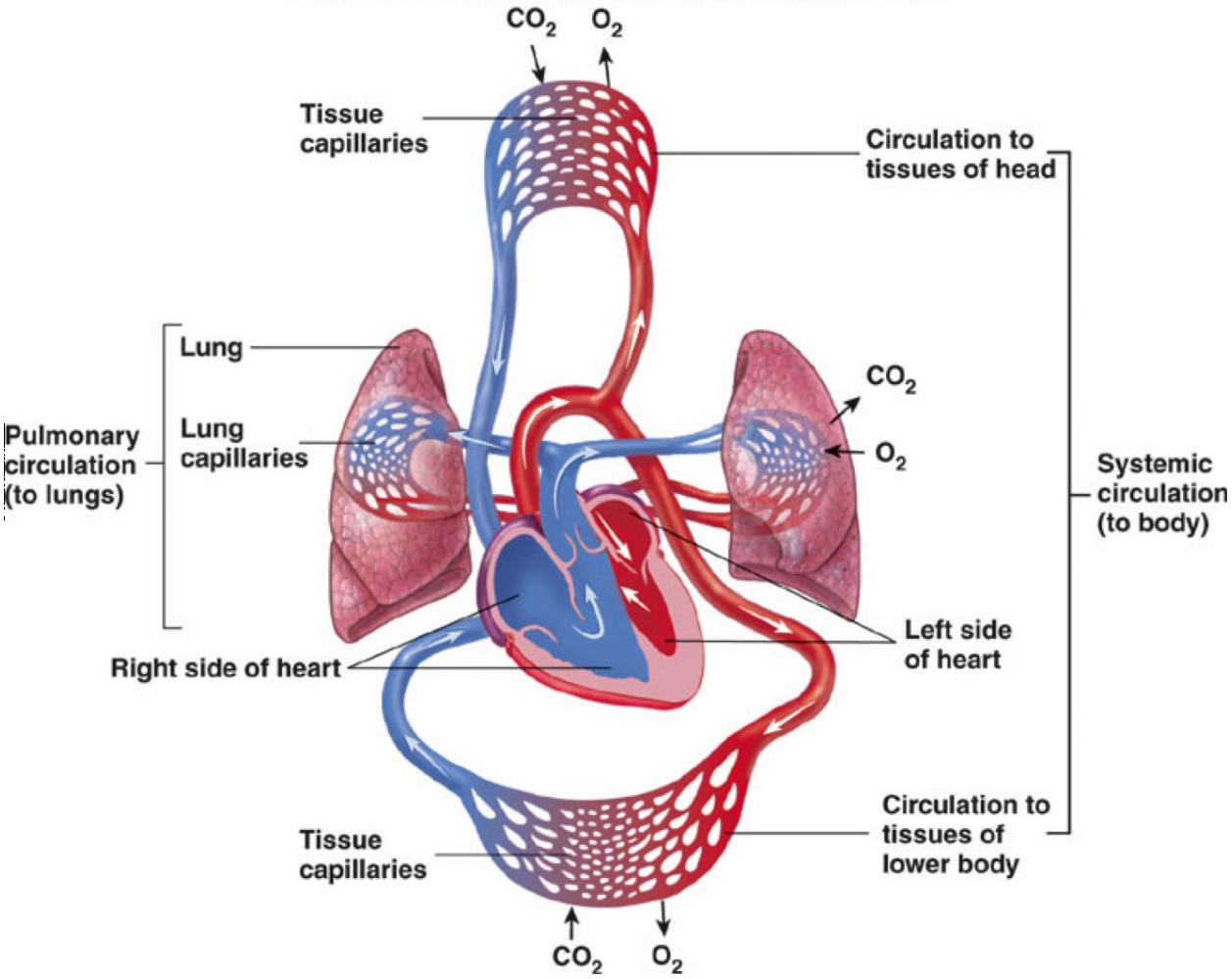

Figure 1.2: The cardiovascular system [3]

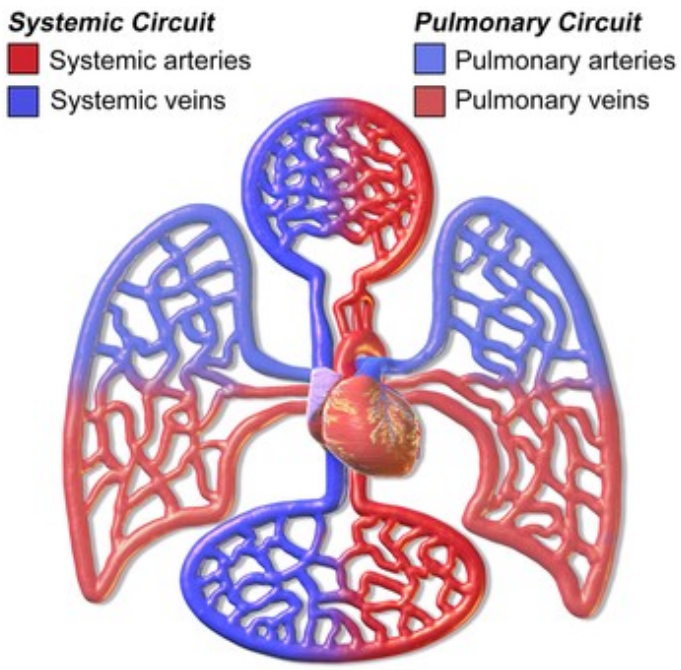

Figure 1.3: The systemic and pulmonary subsystems [4]

The blood going to the right heart will arrive as an inflow of deoxygenated blood that will enter the right atrium of the right heart from two main veins; blood arriving from the upper body will flow through the superior vena cava while the blood from the lower body will enter through the inferior vena cava. This accumulated blood will proceed through the tricuspid valve and enter the right ventricle when it expands. As the right ventricle contracts, this blood is sent through the pulmonary valve and into the pulmonary artery to go to the lungs and get oxygenated. Once the blood is oxygenated, it returns to the left heart via the pulmonary veins. The freshly oxygenated blood will enter the left atrium and continue through the mitral valve and into the left ventricle. When the left ventricle contracts, blood will travel through the aortic valve and into the aorta where it will get distributed to the various organs and muscles of the body.

It should also be mentioned that the heart is characterized as being a double pump since each side, although timed with respect to each other, act as two separate pumping systems. The time

period for the expansion of the heart, in order to fill up with blood, is called *diastole* while the time period for its contraction, so as to pump out the blood, is called *systole*. Same as with the two sides of the heart, both diastole and systole are functionally independent yet they are related to each other based on the principle of conservation of mass of the blood being pumped. It goes without saying that the malfunctioning of this system would lead to seriously detrimental consequences to one's health therefore reinforcing the importance of research regarding the cardiac system.

What makes this field particularly large is due to the great number of causes and locations where a heart can improperly work. Everything from the malformation of a wall to the blockage of an artery creates a need for research into the causes and the solutions for treatment.

1.2 The Tricuspid Valve

The atrioventricular valve, more commonly known as the tricuspid valve, is the barrier between the right atrium and the right ventricle [5]. The flow of deoxygenated blood travels from the right atrium and into the right ventricle by ways of the tricuspid valve, which regulates its inflow. Its name originates from the fact that it is composed of three cusps which house three leaflets that overlap each other when the valve closes in order to create a leak-proof seal. The closure line between the leaflets is referred to as a commissure. Additionally to the cusps, the tricuspid valve has three supporting structures named the annulus, the chordae tendineae and the papillary muscles [6]. The annulus is an elliptical shaped structure formed by the bases of the three leaflets. It helps in maintaining the overall shape and placement of the leaflets. The papillary muscles secure the tricuspid valve into place while the chordae tendineae prevent the valve from inverting into the atrium [7].

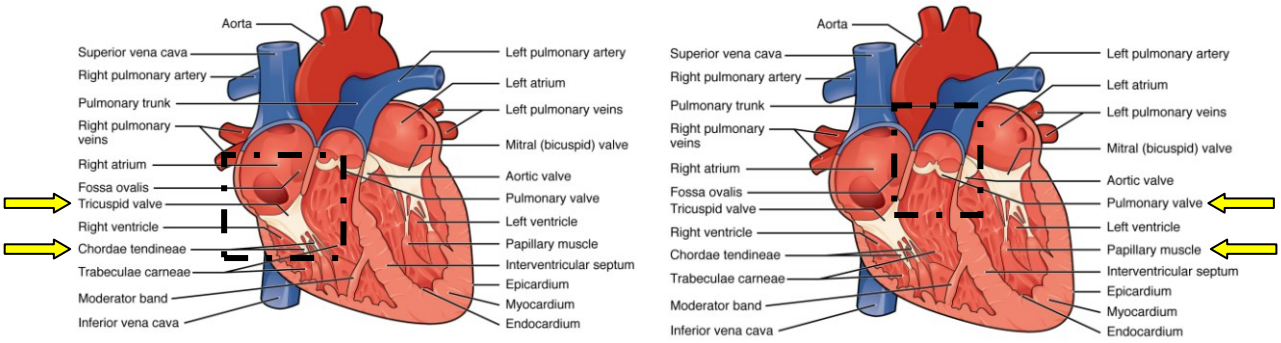

Figure 1.4: (a) Anterior view of the tricuspid valve, (b) Anterior view of the pulmonary valve [8]

This unidirectional valve only opens once the pressure in the right atrium is sufficiently higher than the pressure in the right ventricle and will remain open until the pressure drops.

1.3 The Pulmonary Valve

The pulmonary valve is the barrier between the right ventricle and the pulmonary artery. Similar to the tricuspid valve, this valve is composed of three cusps, however, they are semilunar in shape. Furthermore, unlike the tricuspid valve, the pulmonary valve has a coaptation region in the center of the valve named the corpus arantii. Although commissures are also present, the coaptation region is where the leaflets, of slightly different sizes, overlap in order to prevent regurgitation into the right ventricle [7]. The coaptation surface, or overlapping tissue, is known as the lunula. The pulmonary valve can be seen in Figure 4 (b).

It is a unidirectional valve that allows the flow of deoxygenated blood from the right ventricle into the pulmonary artery where it will be taken to the lungs to get oxygenated.

1.4 Tetralogy of Fallot

This particular research focuses on a congenital heart defect called tetralogy of Fallot. This condition is a multi-defect condition since it encompasses four different defects that manifest themselves at the same time in a child's heart.

- The first main defect is referred to as pulmonary valve stenosis. In essence, it is the narrowing of the pulmonary valve connecting the right ventricle to the pulmonary artery, which is the main artery leading to the lungs. This narrowing causes a smaller amount of blood to reach the lungs and hence, a smaller amount of oxygenated blood reaching the rest of the body.
- This leads to the second defect called right ventricular hypertrophy. Since the heart is in essence a muscle that continuously contracts and relaxes, its wall in the right ventricle will experience thickening due to its needs to overwork to compensate for the lower blood flow due to the stenosis.
- The third defect is the ventricular septal defect where an opening between the two lower heart chambers, known as the ventricles, allows the oxygenated blood in the left ventricle to mix with the deoxygenated blood in the right ventricle. This also contributes to the right wall hypertrophy since the optimal pressure for chamber emptying is never reached.
- The last defect is the overriding aorta where instead of the aorta lying on top of the left heart, it is directly on top of the septal defect, meaning that it receives a mixture of both oxygenated and deoxygenated blood and relays it to the rest of the body. These defects can be visualized in Figure 5.

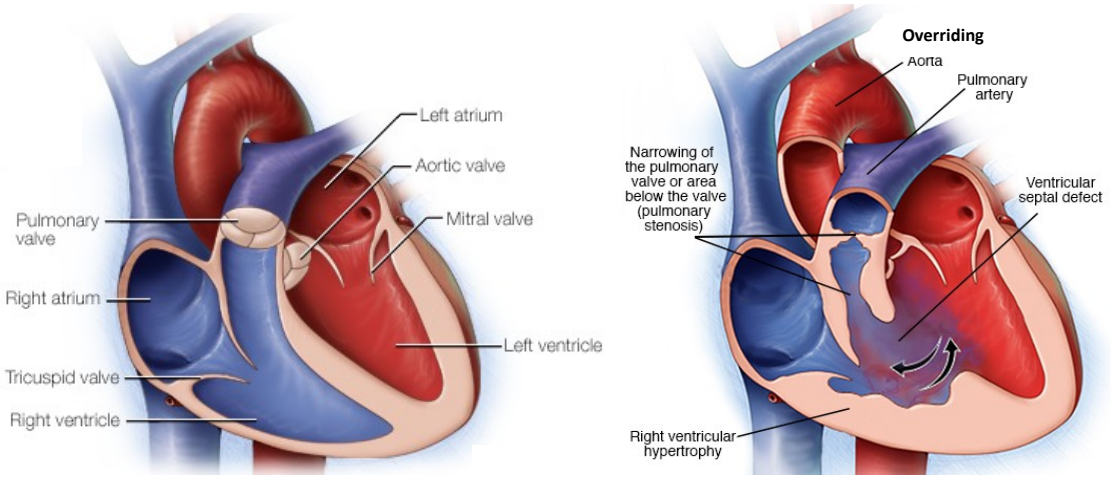

(a) **(b)**

Figure 1.5: (a) Normal heart anatomy [9], (b) Tetralogy of Fallot defects [10]

This condition was chosen since it accounts for 8-10% [11] of all detected defects [12], making it the most common cyanotic defect. Approximately 1 in 2518 births will result with tetralogy of Fallot, leading to about 1657 cases per year in the United States alone [13]. Since this is a congenital defect, all of those affected will need surgical repair at, or soon after, birth in order to have a relatively normal life and longer life span. Since 1955, the surgery required for the repair has become quite indispensable since it reduces mortality by approximately 50% [12, 14]. Unfortunately, pulmonary regurgitation has been observed to appear 2 to 3 decades after the initial operation [15, 16, 17, 18] in 50% of operated cases [12, 17, 19, 20]. It is also to be expected that as time elapses from the initial operation, there are higher probabilities that re-intervention is necessary [13]. Although it is quite possible to live with this condition, about 37% of these cases will need pulmonary valve repair [12, 17, 19, 20]. The cause of this complication has yet to be determined but it will entail several serious sequelae such as right ventricular dilation, impairment of right ventricle function, deterioration of exercise capacity, arrhythmias, and elevated risks of morbidity and mortality [12, 21, 22, 23, 24, 25, 26, 27, 28, 29, 30, 31, 32,

33, 34, 35, 36, 37]. There are however, determinants that are constantly observed with pulmonary regurgitation and that can be used in the determination of the severity, such as the regurgitant orifice area, the duration of the diastole, the ventricular diastolic compliance, and the pressure gradient between the artery and the ventricle [16, 29, 32, 38].

Given that not much is understood about how these consequences come to be, this thesis aims at experimentally evaluating the flow dynamics in the right ventricle. Several cases with various degrees of regurgitation will be simulated and planar time-resolved particle image velocimetry will be applied to the right ventricle. This will be the first experiment of its kind given the complex shape of the right ventricle. The results of such an experiment could potentially yield new parameters that could be used in determining the severity of pulmonary regurgitation in patients.

1.4.1 Pulmonary Stenosis

Pulmonary stenosis is, in this instance, a congenital defect and not a developing condition. It is characterized by an obstruction to the blood flow from the right ventricle to the pulmonary artery. This obstruction is caused by narrowing which more commonly occurs at any of these three locations or combination of locations; either the muscle below the pulmonary valve thickens, the pulmonary artery right above the valve thickens, or the valve leaflets themselves thicken and fuse together along their separation lines, which would cause the leaflets to become less pliable [39]. It is also possible for the valve itself to be of smaller diameter, allowing less blood flow through.

In the case of tetralogy of Fallot, the stenosis occurs primarily at the valve, which is specifically called pulmonary valvar stenosis. In some instances, this obstruction can additionally affect the muscles below the valve and in some rare cases, the valve may not even fully form (pulmonary

atresia) [40]. The considerable decrease in blood flow will result in less oxygen circulating throughout the body and will cause the right ventricle to overwork in order to compensate for the deficiency.

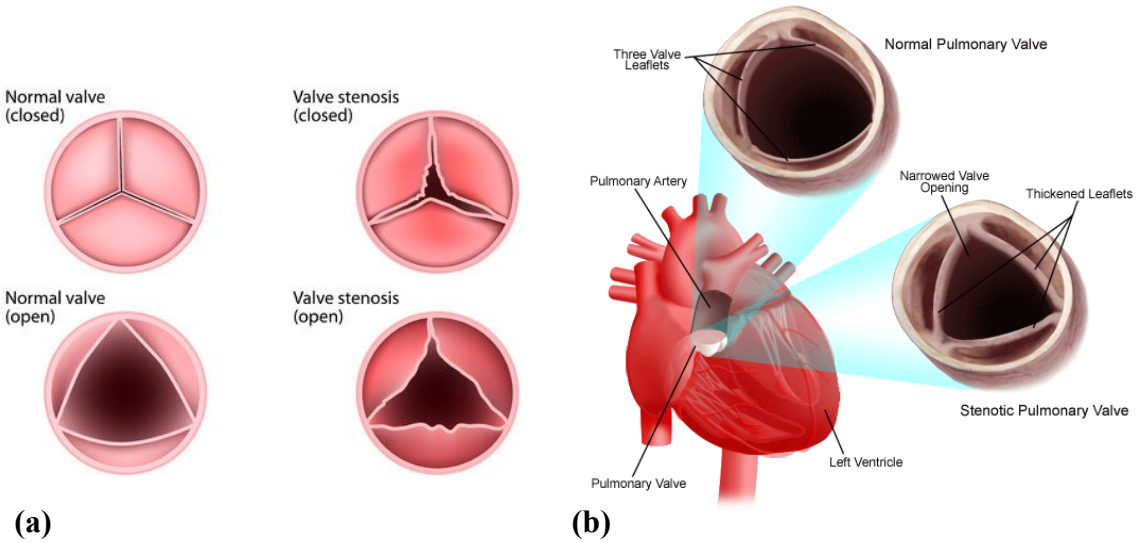

Figure 1.6: (a) Normal and stenotic pulmonary valve [41], (b) Further example of normal and stenotic pulmonary valve [42]

1.4.2 Right Ventricular Hypertrophy

Hypertrophy is the medical term used for the enlargement of a muscle. In this context, the heart of a patient with tetralogy of Fallot will undergo hypertrophy, predominantly on the right side.

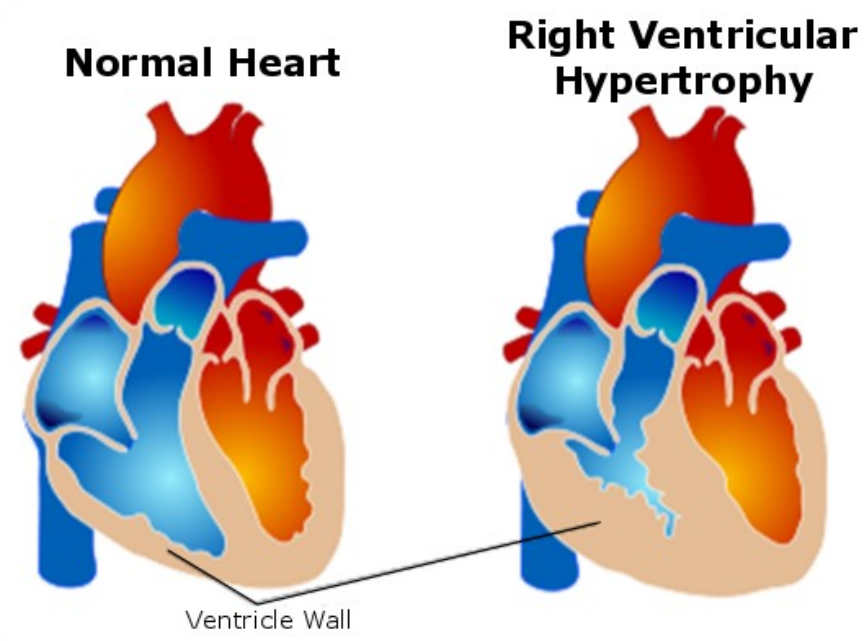

Figure 1.7: Right ventricular hypertrophy [43]

This occurrence is due to the presence of the other three defects. First, the stenosis at the pulmonary valve restricts the exit of blood flow from the right ventricle to the lungs. This signifies that a decrease in blood volume is being oxygenized and sent to the remainder of the body. In order to compensate for it, the right ventricle will pump more frequently and increase the heart rate in order to increase the amount of oxygenized blood to the body. Second, the ventricular septal defect allows the passage of blood between the two ventricles, which hinders the proper functioning of the heart. Due to this opening, deoxygenated blood from the right ventricle flows into the left one, decreasing the amount of blood pumped to the lungs to get oxygenated. Additionally, oxygenated blood moves to the right ventricle and gets sent to the lungs, making the process very inefficient. The overall effect is that the right ventricle needs to pump a lot more in order to cater to the oxygen demand of the entire body. Third, the overriding aorta send a mixture of oxygenated and deoxygenated blood to the body, further increasing the demand for oxygen from the body. The combination of these three defects causes the right

ventricle to work harder in order to compensate for them. As an end result, the heart becomes very weak and stiffens, which may lead to failure and cardiac arrest.

1.4.3 Ventricular Septal Defect

Ventricular septal defect can only be congenital and does not develop over time. In essence, it is the lack of a fully formed septal wall between the right and left ventricles of the heart. Although a septal defect could also occur in between the two atria, named atrial septal defect, the only location associated and observed in tetralogy of Fallot patients are in the ventricular region. There are four main ventricular septal defects that could occur:

- **conoventricular ventricular septal defect**: in this instance, the hole forms just beneath the pulmonary and aortic valves.
- **perimembranous ventricular septal defect**: the hole occurs in the upper area of the ventricular septal wall.
- **inlet ventricular septal defect**: the hole occurs near where the blood inflow from the tricuspid and mitral valves.
- **muscular ventricular septal defect**: this hole occurs in the lower region of the ventricular septal wall, where it is surrounded by muscle tissue.

The ventricular septal defect most commonly seen in tetralogy of Fallot patients is the conoventricular septal defect which, due to its location, is a factor in the narrowing of the right ventricle outflow tract (i.e., pulmonary stenosis) [11]. In some instances, the opening can be minor and could repair itself, however, tetralogy of Fallot patients typically have an opening large enough that it needs to be addressed surgically near birth. The severity of this can be quite

high since the deoxygenated blood from the right ventricle is allowed to enter and mix with the oxygenated blood of the left ventricle, which is to be pumped to the body. This signifies that organs and cells of the body will receive a lower amount of oxygen than required. Similarly, the oxygenated blood of the left ventricle will enter and mix with the deoxygenated blood of the right ventricle, which is to be sent to the lungs. This makes the circulation of oxygenated blood very inefficient. Additionally, since insufficient oxygen is being sent to the body, the heart attempts to pump a higher amount of blood in order to compensate. Needless to say, this results in the heart overworking and leads to its weakening or in some instances, failure.

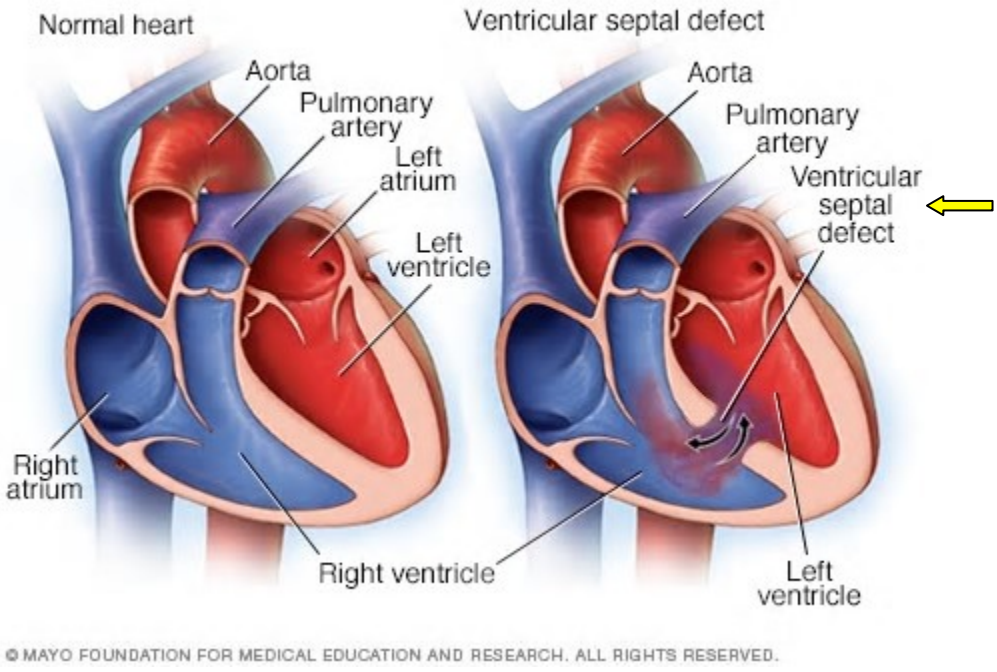

Figure 1.8: Ventricular septal defect [44]

1.4.4 Aortic Displacement

Aortic displacement or overriding aorta is the last of the four defects. The normal placement of the aorta is branching off the top of the left ventricle. Blood flow is regulated by the aortic valve, over which the aorta resides. Aortic displacement occurs when the aorta is slightly displaced and rests right above the ventricular septal defect. Due to its abnormal placement, the aorta transports a mixture of oxygenated and deoxygenated blood to the body since the septal defect allows for blood mixture. This is yet another defect, which causes the distribution of oxygen-poor blood to the body, further contributing to cyanosis, the bluish tint of the skin.

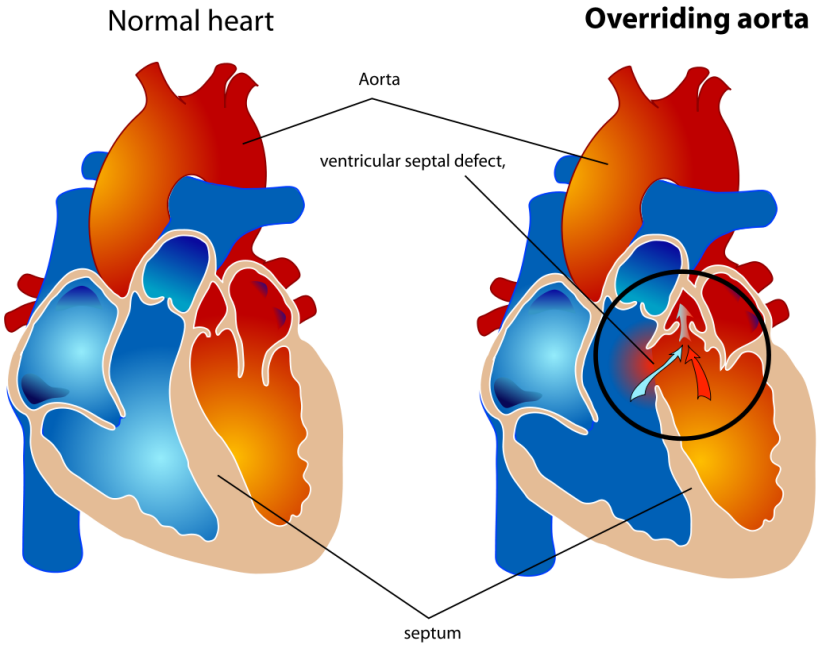

Figure 1.9: An overriding aorta [45]

1.5 Tetralogy of Fallot Surgery

1.5.1 Complete Intracardiac Repair

In the majority of cases, surgery is required to repair the defects which could have life threatening results if left untreated. Of the four defects, only two need to be mended in order to have an adequately functioning heart; The pulmonary stenosis and the ventricular septal defect.

The pulmonary stenosis is repaired through several minor mends. First, the pulmonary blood vessels are widened. Then, the pulmonary valve is either widened or entirely replaced by either a mechanical or biological prosthetic valve. Lastly, the passage between the right ventricle and the pulmonary artery is enlarged. All of these repairs allow for better and more effective blood flow to the lungs.

The ventricular septal defect is simply repaired by applying a Dacron patch [46] to the opening. By doing so, blood can no longer travel between the right and left ventricles.

With the repair of the two aforementioned defects, there would be no worry of the aorta transporting a mixture of oxygenated and deoxygenated blood. Additionally, the restoration of proper blood flow in the right ventricle will alleviate the excess load on the ventricle and eliminate the hypertrophy [47].

1.5.2 Palliative or Temporary Surgery

It occurs in some instances that the infant is simply not strong enough to endure a surgery as previously described. In this case, a temporary surgery could be performed within the first few months after birth in order to help the child increase blood oxygen levels until he/she is strong enough to withstand the complete repair surgery. This temporary surgery simply consists of attaching a shunt between the aorta and the pulmonary artery. A shunt, which is basically a tube,

will allow the blood to flow from the aorta and into the pulmonary artery in order to get oxygenated. Depending on the circumstances of the patient's situation, there are four different shunts that can be inserted; a classic Blalock-Taussig shunt, a modified Blalock-Taussig shunt, a Watertson shunt, or a Potts shunt.

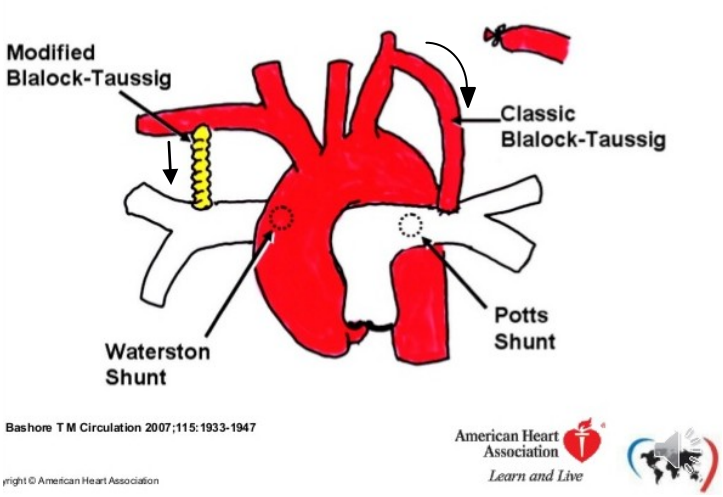

Figure 1.10: Various shunts for palliative tetralogy of Fallot surgery [48]

This procedure will aid the infant in producing oxygen rich blood in order to cater to his/her body's needs. Once the child has grown sufficiently and is stronger health-wise, the shunt is removed and the complete repair surgery is performed [47].

1.6 Pulmonary Valve Regurgitation

As mentioned previously, pulmonary valve regurgitation often occurs 2 to 3 decades after the initial tetralogy of Fallot repair surgery. It is, in essence, when blood in the pulmonary artery flows backwards into the right ventricle, therefore increasing the volume of blood contained in the ventricle. This is due to the pulmonary valve not being able to close adequately; since the leaflets do not close properly and form a sealed surface, blood is allowed to flow backwards.

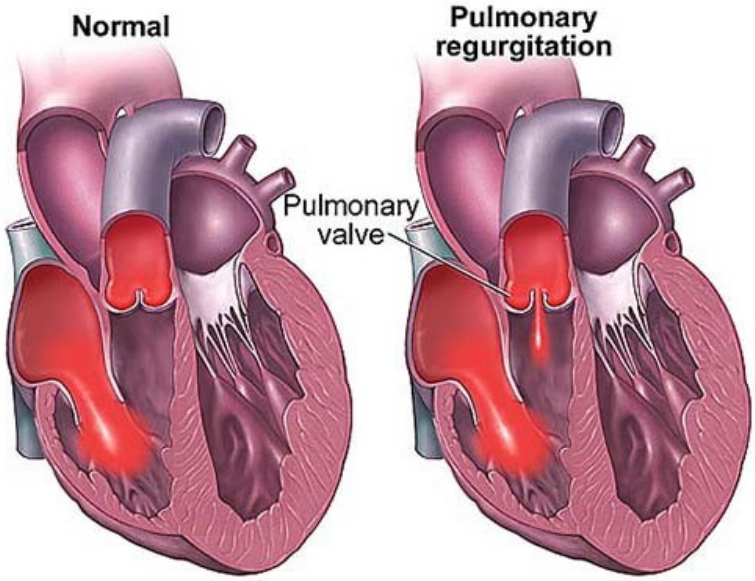

Figure 1.11: Pulmonary regurgitation [49]

Although it is not quite understood why this occurs, 50% of patients do need a valve replacement operation. What makes this occurrence tricky is that it is not always detectable. There is a specific heart murmur that doctors need to catch, often named a Graham-Steele murmur [50], in order to detect it. If it is not caught early, the right ventricle might end up enlarging. In extreme cases, heart failure might occur, however, more noticeable symptoms such as chest pain will alert the patient that something is amiss [51].

1.7 Pulmonary Valve Replacement

Although mild regurgitation can be managed without any surgical interference but simply with supervision, moderate and severe cases will in most instances require a surgical intervention at the discretion of the patient's doctor. Valve repair is the preferred solution to a malfunctioning valve since it maintains the valve's strength and function, eliminates the need for blood thinning

medications and significantly decreases the risk of infection [52]. In the event that the regurgitation is too severe, valve replacement will have to be performed. Depending on several factors such as age, overall health and individual circumstances, surgeons will have to choose between a mechanical or biological prosthetic valve, but neither is without its own issues. Although bioprosthetic valves are widely liked since they are the most similar to the original biological valves, mechanical valves are typically favored for patients under the age of 60 due to their durability [53]. Bioprosthetic valves allow for a blood flow similar to that observed with the original valve, however, no *in vivo* studies show that they maintain proper vortex formation. Additionally, bioprosthetic valves have a degeneration rate inversely related to the age of the patient at the time of implantation, making it more favorable for elder patients above the age of 60 [54]. Alternatively, mechanical valves carry with them the necessity of anti-coagulation medications as well as the elevated risk of thromboembolism (blood clot from another area that has traveled and blocked the artery), which may lead to a stroke or arterial thrombosis (blood clot formation in the artery) [53].

Chapter 2 - Literature Review

2.1 Overall Tetralogy of Fallot Repair and Repercussions

The repair of tetralogy of Fallot is deemed as one of the most important advances made regarding the repair of a congenital heart defect. However, the effects of the complications occurring after the initial repair on the ventricle still remain a mystery as well as the reason for their appearance. To reinforce the importance of this dilemma, several published articles refer to the importance of further investigations, as well as the work already accomplished by the scientific community. For instance, Zaragoza-Macias and Stout [13] showed that although the success of the initial repair is undeniable with a reduction in mortality of about 50%, there remains a considerable percentage of 37% of these survivors who will need pulmonary valve replacement due to the regurgitation present with the current valve. The second issue raised in this paper is regarding the optimal timing for the valve replacement operation. There is currently no way of gauging when is the ideal time to perform this operation, therefore, it is necessary for scientists to conduct further tests and observations on patients after they have undergone the valve replacement procedure. These same conclusions were reached by Yoo And Park [16] during their research. They have found that instead of doing an aggressive reconstruction of the right ventricle in order to relieve pulmonary stenosis, it was overall better long-term for the patient to receive conservative right ventricle reconstruction at the expense of residual pulmonary stenosis. Doing so creates a lower risk of right ventricle deterioration when pulmonary regurgitation occurs. However, once again, it is emphasized that further research into the flow dynamics inside the ventricle is necessary in order to fully comprehend these complications.

Hickey et al. [15] went more into detail when trying to determine the functional health of adults who had survived the initial repair of tetralogy of Fallot. Their research yielded that there is only about a 1% risk of needing another operation each year after the initial repair. However, this percentage increased once the patients reached 40 years of age. Furthermore, about 54% of all patients exhibited moderate to severe regurgitation and one third of patients had pulmonary stenosis present. Once again, these numbers only reinforce the underlying issue that there is a need for a further extensive understanding of the right ventricle functioning in order to properly address this defect.

2.2 Regurgitation Quantification

There are several ways to go about trying to understand the functioning of the right ventricle and the effects of regurgitation towards it. One of the approaches tackled was to try to refine the method with which regurgitation is measured. Wald et al. compared two main ways of quantifying pulmonary regurgitation; either by volume or by fraction. Their results showed that it may be overall more accurate to use a volumetric measurement [28].

On the other hand, other scientists have determined a strong correlation between the regurgitation fraction and the orifice present in the pulmonary valve. Furuse et al. have shown that aside from the aforementioned relation, their observations depict a trend where the right ventricle is able to sustain a certain amount of pulmonary regurgitation. The increase in volume did not compromise the functioning of the ventricle and an adequate outflow from the ventricle was seen. Additionally, they determined that this is only true until the regurgitation fraction reaches about a 15% threshold, at which point the right ventricle no longer works adequately [55]. It is interesting to note that between the usage of volume and fraction as a method of

measurement for regurgitation, the fractional method is more prevalent although the volumetric method might be deemed more accurate.

2.3 Velocity Fields and Flow Structures in the Right Ventricle

Even though it has been numerously repeated that there is practically no certain knowledge of the flow present in the right ventricle, there is one structure that has been shown to be crucial in the proper functioning of both ventricles. Pedrizzetti et al. confirmed that vortices are an intrinsic part of the proper functioning of ventricles. Moreover, the change in vortex dynamics is linked to physiological changes in the heart. It should be noted that the exact nature of these changes isn't restricted to one type and that the main conclusion of this study is that the behavior of the vortices are an accurate determinant of cardiac malfunctioning [56].

The importance of vortices in the right ventricle is also underlined in the work done by Pasipoularides et al. They showed that inflow jet from the tricuspid valve followed the endocardial wall and descended towards the apex to then continue following the wall upwards. This resulted in the clear formation of counter-clockwise vortex motion during diastole in a normally functioning heart [57]. These findings were further supported by ElBaz et al. who showed that not only is there formation of a vortex ring during the E-filling phase but there also one formed during the A-filling phase [58]. Naturally, it is once again emphasized that further research regarding the hemodynamic flows in the ventricles is necessary.

2.4 Visualization Methods

Aside from using particle image velocimetry to visualize fluid flow in the ventricle, other means have been explored in the past few years. The most popular of these methods is using

magnetic resonance imaging, its usage most prevalent in health care facilities. An up runner to this method is the Doppler echocardiography. Several studies have been performed in order to compare the effectiveness and accuracy of these methods. There seems to be unanimous agreement between the three studies of Li et al., Grothoff et al., and Festa et al. that the usage of Doppler echocardiography is an acceptable and efficient way of visualizing the cardiac flow and determining the severity of pulmonary regurgitation. Additionally, this method is non-invasive, a criteria that is particularly attractive in healthcare and research [59, 60, 61].

A relatively recent method more related to the usage of particle image velocimetry was explored by Falahatpisheh et al. They were able to obtain a three-dimensional flow field of the cardiac chambers by superimposing multiple perpendicular two–dimensional flow fields. Furthermore, this method was validated through numerical and analytical methods [62].

2.5 Viscous Energy Losses

Viscous energy dissipation is a parameter that has been gaining popularity in the past few years. It used to be a measurement difficult to acquire, however, with today's technology and methods, it is relatively easy and non-invasive to acquire from a patient. Akins et al. claim that the energy loss is the new parameter on which clinicians must focus on in order to better diagnose and treat their patients. They state that by evaluating the energy loss in a ventricle, valve performance, be it native or prosthetic, can be gauged. It goes without saying that poor valve function will have negative effects on proper ventricle functioning [63]. Such statements are supported by Shibata et al.'s work. Their aim was to show that by using flow energy loss, right ventricular deterioration due to pulmonary regurgitation after tetralogy of Fallot repair could be predicted. By achieving this, a more appropriate timing for pulmonary valve

replacement could be accomplished while potentially avoiding any deterioration of the right ventricle. By monitoring patients who had undergone tetralogy of Fallot repair, they were successful in demonstrating how flow energy loss is indeed useful in predicting right ventricular deterioration. Their results showed that although there was not a positive correlation between the severity of pulmonary regurgitation and the flow energy loss, there was still a significant correlation between the flow energy loss and the cardiothoracic ratio. In other terms, the amount of flow energy loss is not necessarily indicative of the severity of the pulmonary regurgitation but if the size of the heart compared to the thoracic cavity were to increase or decrease, then the flow energy loss will also increase or decrease respectively. Further positive correlation were found regarding other parameters such as the QRS complex. Although regurgitation does play a role in right ventricular deterioration due to the presence of turbulence, it simply does not seem that energy loss is significantly correlated to the severity of the regurgitation. Nonetheless, one must bear in mind that these results are only meant for mid-term outcomes and not for long-term ones [64].

Viscous energy dissipation has been examined in the right ventricle in order to study effects from various pathologies, however, there is a clear inclination towards measurements taken in the pulmonary artery. Seldom are there experiments undertaken in the right ventricle itself, making this experiment all the more novel.

2.6 Proper Orthogonal Decomposition

Proper orthogonal decomposition has been accepted and used for a substantial number of years now, considering it was first introduced in the 1960s by Lumley [65], it does not seem to have been applied very often on the right ventricle after the repair of tetralogy of Fallot or in the

field of cardiovascular flows for that matter. Granted, it has been applied to investigate pathologies such as hypertension [66], but once again considerably more experiments have been conducted on the left ventricle. For instance, Di Labbio and Kadem [78] used proper orthogonal decomposition when reconstructing the flow present in a healthy left ventricle of the heart as well as to reconstruct the flow when aortic valve regurgitation was present. Their results showed that the modes generated by POD were quite accurate and were effective in reproducing the velocity gradients.

More commonly, proper orthogonal decomposition has been used as a method to simulate fluid flow through the right ventricular outflow tract in order to better design artificial devices. Caiazzo et al. used proper orthogonal decomposition to help design a reducer stent for tetralogy of Fallot patients who have enlarged right ventricular outflow tracts and therefore are not able to have a suitable bovine or artificial valve implanted in the event of an incompetent or missing native valve. Their results showed that even when using POD, the main flow characteristics were preserved and the observed errors regarding forces on the devices and flow rates were below 6% [67].

As another example, Guibert et al. created an average pulmonary artery geometry from 17 tetralogy of Fallot patients through which blood flow was simulated and POD was applied. The obtained POD is then a basis with which mapping can be done on new patients in order to perform reduced order blood flow simulations with patient specific boundary conditions. Naturally, the mapping was also done on the 17 initial population and results showed that this method yielded acceptable error margins and the POD held quite well in the face of changing boundary conditions [68].

The lack of experiments regarding the overall flow in the right ventricle signifies that the experiments conducted for this thesis are also novel with respect to this front and with their results hopefully shedding light on the prevalent fluid structures and flows in the right ventricle after the repair from tetralogy of Fallot.

Chapter 3 - Methodology

3.1 Overview

Since this experiment only looks at the fluid structures in the right ventricle, it then goes without saying that only certain components of the cardiovascular system are studied, namely; the right ventricle, the right atrium, the tricuspid valve, the pulmonary valve, and the pulmonary artery. All of the aforementioned cardiac components, except for the valves, are molds made out of silicone such that certain of their anatomical characteristics and deformations can be duplicated. This is crucial in regards to the pressure since lack of compliance will result in a pressure non-representative of an actual cardiac system. The overall experimental setup is a double activation heart simulator which enables one to simulate the functioning of a human heart. The contractions of the right ventricle were regulated through the use of a piston cylinder assembly alongside a linear motor which changed the pressure in the hydraulic activation chamber where the ventricle was located. This motor gave rise solely to the systolic E-wave. Additionally, a servomotor was installed above the atrium in order to obtain an adequate diastolic A-wave. Two tri-leaflet porcine valves were used to replicate the tricuspid valve and the pulmonary valve (25 mm St-Jude Medical (SJM) porcine valve). A sketch representing the experimental setup can be observed in Figure 12 as well as a picture of the activation chamber containing the ventricle in Figure 13.

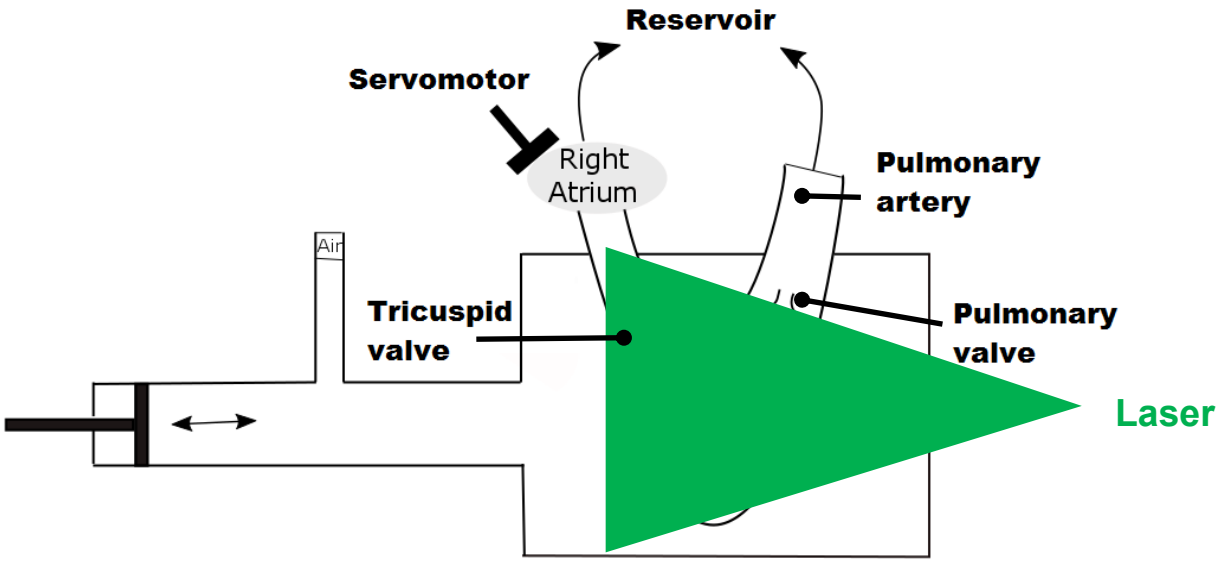

Figure 3.1: Schematic representation of the experimental setup

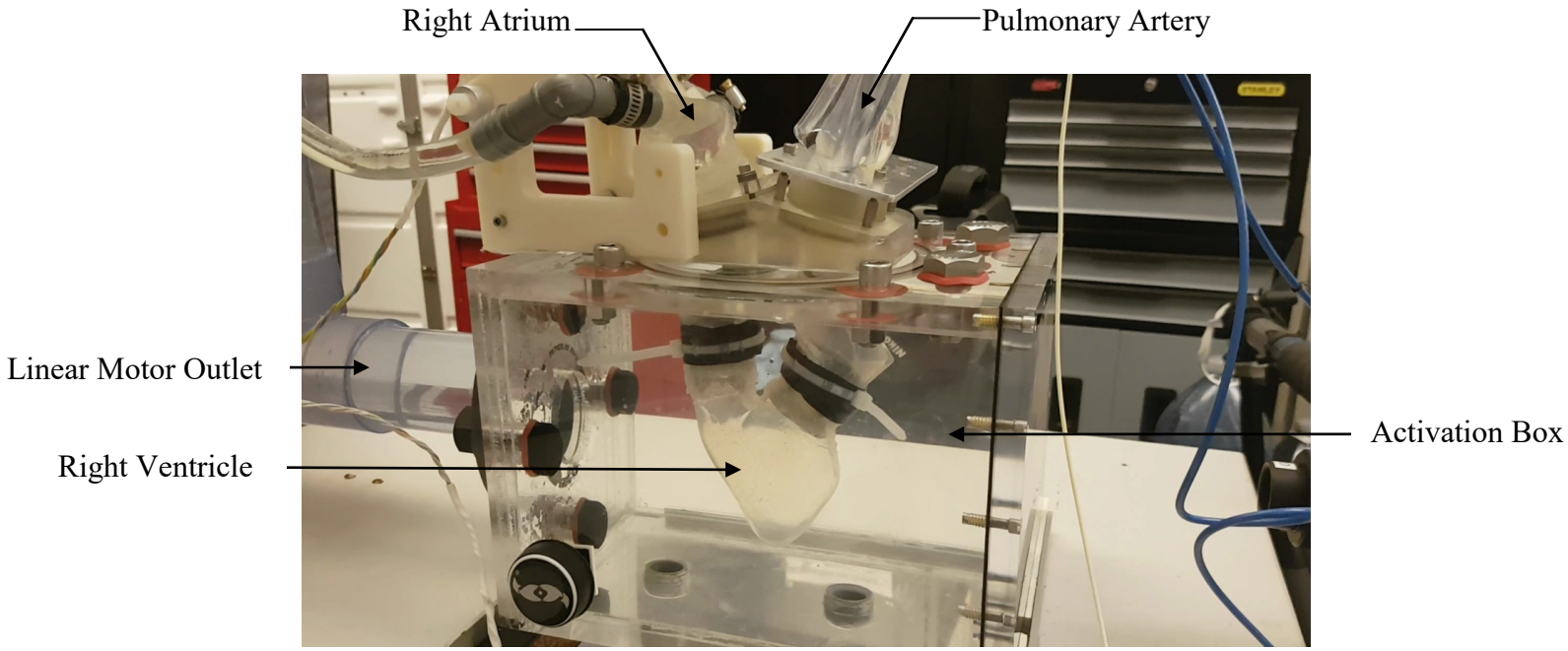

Figure 3.2: Picture of activation chamber containing the right ventricle

3.2 In Vitro Setup

The experimental setup used in this study was custom made to accommodate the silicone molds used. The system can be represented by a circuit where the origin point is a water reservoir tank located at a higher elevation than the cardiac components. This elevation allows for the flow of the blood duplicate since no pump was incorporated in this setup. From this tank, a pipe carries the water-glycerol mixture (dynamic viscosity of 4.2 x 10^{-3} Pa·s and density of 1100 kg/m^3) until it divides into the two inlets of the right atrium. The servomotor at this location then helps the water mixture to enter the right ventricle through the tricuspid valve and the simulated heart contractions push the mixture out of the ventricle, through the pulmonary valve and into the pulmonary artery. Therefore, as mentioned previously, the linear motor will give rise to the E-wave while the servomotor gives rise to the A-wave. The pipe representing the pulmonary artery extends until it reaches back to the initial tank, hence creating the circuit.

The water-glycerol mixture was chosen primarily for two of its attributes. First, this mixture offers a good approximation of the dynamics blood would have since its dynamic viscosity (4.2 x 10^{-3} Pa·s) is quite close to that of human blood (4.4 x 10^{-3} Pa·s ± 0.6 x 10^{-3} Pa·s) [69] at a normal body temperature [70]. Although it is true that blood behaves as a non-Newtonian fluid, studies have shown that due to the high shear rates observed in the heart chambers and large arteries, it can be considered a Newtonian fluid in such locations [71, 72, 73]. This additionally justifies the use of the water-glycerol mixture since an actual non-Newtonian fluid is not necessary.

The second reason for this choice of medium is its refractive index. In order to effectively perform particle image velocimetry, a clear fluid must be used in order for the laser to go through and refract on the particles used. Additionally, this refractive index is the same as that of the

silicone molds used in the experiment, making it the perfect choice so that the laser sheet is not distorted between the mixture and molds.

3.3 Silicone Molds

As aforementioned, the anatomical components of this system are made out of a silicone mixture (MB Fiberglass Polycraft T-4 Translucent silicone Rubber 1.1kg kit). These molds were created by painting layers of the said mixture on an accurate 3D-printed cavity model. Depending on the elasticity required, differing number of layers were used for each component. The characteristic elasticity of the heart which allows it to efficiently contract was simulated by painting three layers of the silicone mixture, while the stiffer pulmonary artery required five. In all cases, the silicone is created by mixing with a 10:1 ratio, silastic T-4 base to silastic T-4 curing agent. This particular silicone has a tensile strength of 6.7 MPa and can reach an elongation of 400% at failure. Furthermore, it has a tear strength of 26 N/mm and a refractive index of 1.39.

3.4 Experimental Conditions

Regurgitation through the pulmonary valve was achieved through the restriction of the leaflets' closing. By doing so, four cases with varying severities were created and studied: (1) normal, (2) mild, (3) moderate, and (4) severe. All of the previously mentioned cases are defined by ratio of the effective regurgitant orifice area over the total valve orifice area (ROA/A); (1) the normal case has no regurgitant orifice (0 ROA/A), (2) 0.012 ROA/A for the mild case, (3) 0.063 ROA/A for the moderate case, and finally (4) 0.174 ROA/A for the severe case. Since there is no presence of clinical guidelines for severity categorization for pulmonary regurgitation in literature, these orifice areas are not representative, nor do they simulate *in vivo* cases. Instead,

these regurgitant orifices were selected in order to effectively demonstrate the development of the fluid flow in the right ventricle when pulmonary regurgitation is present. The pressure in the pulmonary artery was measured with a Millar MPR probe (Millar Instruments, Houston, TX, USA, SPC 360S, accuracy 0.5 % full scale) placed in the artery itself, near the exit of the pulmonary valve. Flow rate in the pulmonary artery was measured using a Transonic transit-time ultrasonic flow meter (T206 Series with A-probes, Transonic Systems Inc.; Ithica, NY). In all of these cases, a heart rate of 70 beats per minute was maintained alongside a flow rate of 4.2 L/min. A more extensive summary of the experimental conditions can be found below in Table 1.

Table 1: Summary of working fluid properties and operating conditions
(where $\boldsymbol{Wo = R\sqrt{\frac{n\rho}{\mu}}}$ [74], *n* being the angular frequency, *R* being the radius)

Working fluid properties *		**Operating conditions**	
Density (*ρ*)	1100 kg/m^3	**Cardiac output**	4.2 L/min
Water- Glycerol ratio	60-40 (by volume)	**Cardiac cycle period**	0.857 s
Dynamic viscosity (*μ*)	0.042 Pa.s	**Heart rate**	70 bpm
Refractive index	1.39	**Womersley number (Wo)**	13.14

* at 23°C

3.5 Particle Image Velocimetry System and Settings

A LaVision system (LaVision GmbH, Goettingen, Germany) with a dual cavity Nd: YLF laser (Litron lasers, Warwickshire, England) was used for this experiment. A maximum repetition rate of 20 kHz can be achieved as well as a maximum pulse energy of 10mJ at 527 nm. Alongside the PIV system, a Phantom v9.1 camera (Vision Research, Stuart, FL, USA) equipped with a Nikon camera lens AF Micro-Nikkor 60 mm f2.8D was used in order to get precise

imaging of the flow. This camera is able to obtain 1016 frames per second (508 double frame) with a maximum resolution of 1632 x 1200 pixels. The PIV was performed on the central plane of the right ventricle, in such a way that the flow through both of the valves can be observed. This position was attained by accurately placing the laser with the aid of an articulated arm. The plane of light of the laser, of approximately 1 mm width, was used in concurrence with the addition of polyamide particles (mean diameter of 50 μm, ρ = 1030 kg/m^3). The cardiac cycle had a duration of 0.857 s with 750 μs between pulses. During this cycle, 420 images were taken at a frequency of 490 Hz. All images and data were captured on the DaVis 7.2 sorftware (DaVis 7.2, LaVision GmbH, Germany). Vector fields were obtained by applying cross-correlation to the obtained images. An initial interrogation window of 64x64 pixels with a 50% overlap was used as a preliminary method to eliminate noise, out of bound motion and other undesirable sources of error. A second pass with a smaller interrogation window, 32x32 pixels, was then applied in order to increase resolution and efficiently reduce errors [75]. A more extensive summary of the PIV settings can be found in Table 2.

Table 2: Summary of particle image velocimetry parameters

System	LaVision GmbH, Goettingen, Germany.
Laser	Dual cavity Nd:YLF laser (Litron lasers, Warwickshire, England); maximum repetition rate of 20 kHz; maximum pulse energy of 10mJ at 527 nm.
Camera	Phantom v9.1 camera (Vision Research, Stuart, FL, USA) Frame rate: 1000 fps at a maximum resolution of 1632x1200 pixels.
Particles	Spherical polyamide particles (mean diameter of 50 μm, density of 1030kg/m^3).
Spatial resolution	0.8x0.8 mm
Δt	750 μs
Measurement duration	0.857 s
Post-processing	Cross-correlation with multi-pass. Initial 64x64 pixel interrogation window and a final 32x32 pixel interrogation window with a 50% overlap. Median filtering and 5x5 Gaussian smoothing filtering.

3.6 Measurements

The spatial derivatives were calculated using the noise reducing fourth-order compact Richardson extrapolation [76]. Following is the associated equation:

$$\frac{du}{dx_i} = \frac{1}{A_r} \sum_{k=1,2,4,8} A_k \frac{u_{i+k} - u_{i-k}}{2k\Delta x_i} \quad (1)$$

where A_r and A_k are constants of extrapolation, u is velocity and x is the spatial coordinate.

In the case of a two dimensional flow and using the spatial derivatives obtained from the previous equation, the following equation for the vorticity is expected:

$$\omega = \frac{\partial v}{\partial x} - \frac{\partial u}{\partial y} \quad (2)$$

where *x* and y are the spatial coordinates, *u* is the velocity across the *x*-axis, and *v* is the velocity over the *y*-axis.

The energy loss caused by the viscosity of the blood duplicate is obtained through a custom made Matlab code (codes can be seen here: https://www.gdilabbio.com/matfluids) which uses the following equation [77] as well as the previously obtained spatial derivatives:

$$\mathrm{VED} = \sum_{i,j} \int \frac{1}{2} \mu \left(\frac{\partial \mathrm{u}_i}{\partial \mathrm{x}_j} + \frac{\partial \mathrm{u}_j}{\partial \mathrm{x}_i} \right)^2 \mathrm{dA} \tag{3}$$

where μ is the coefficient of blood dynamic viscosity, u_i is the velocity vector component across the x-axis, u_j is the velocity vector component across the y-axis, and i as well as j are the coordinates of the 2D Cartesian coordinate system.

3.7 Circulation

In the event that vortex rings or vortices are present in the flows examined, circulation, which is the measure of the direction of circular motion, is a useful tool in order to analyze such fluid movements. Based on the calculation of vorticity, circulation can sometimes be represented by a dimensionless quantity. In this research, the measurement was chosen to be presented with respect to time and area, as given by equation below [78].

$$\Gamma = \iint \frac{\partial u}{\partial y} - \frac{\partial v}{\partial x} \, dA \tag{4}$$

3.8 Proper Orthogonal Decomposition

Proper orthogonal decomposition is a well-established model that surfaced at the middle of the last century [79]. In essence, it is an algorithm used on unsteady flows and enables one to differentiate the temporal modes from the spatial modes over a determined amount of time. This method allows for the determination of the dominant coherent structures present based on the

amount of kinetic energy that they contain. Finding these dominant modes might allow one to determine detrimental cardiovascular flows which lead to the malfunctioning of the pulmonary valve.

In order to find the pertinent modes, rearranging the velocity vectors into a matrix is necessary [78, 79, 80, 81]:

$$\mathrm{U} = [u^1 u^2 \dots \dots \dots u^N] = \begin{bmatrix} u_1^1 & u_1^2 & \dots & u_1^N \\ \vdots & \vdots & \vdots & \vdots \\ u_m^1 & u_m^2 & & u_m^N \\ v_1^1 & v_1^2 & \vdots\vdots & v_1^N \\ \vdots & \vdots & \vdots & \vdots \\ v_m^1 & v_m^2 & \cdots & v_m^N \end{bmatrix} \tag{5}$$

The covariance matrix can then be determined and using it, the eigenvalues and eigenvectors can be calculated.

$$\mathrm{C} = \mathrm{U}^{\mathrm{T}}\mathrm{U} \tag{6}$$

$$\mathrm{CG} = \lambda \mathrm{G} \tag{7}$$

The temporal coefficients and spatial modes can be determined by:

$$\text{Spatial:} \quad \phi_i = \frac{\mathrm{G}u^i}{\|\mathrm{G}u^i\|}, \quad i = 1, \dots, N \tag{8}$$

$$\text{Temporal: } g_i^n = \psi^T u \tag{9}$$

Finally, the global entropy can be calculated by [82]:

$$H = -\lim_{N\to\infty} \frac{1}{\ln N} \sum_{k=1}^{N} p_k \ln p_k \tag{10}$$

where N is the total number of modes looked at and p is the energy fraction of the mode.

This dimensionless parameter is useful in indicating to one whether the energy is equally distributed among all of the obtained modes, when H has a value of 1, or whether there is a more weighed energy distribution among the modes. The latter case is represented by the value of H

where the extreme case is depicted by a H value of 0 and all of the energy is only contained in the first mode.

3.9 Statistical Significance

With several regurgitant severities explored, it is important to ensure that the cases are varied enough such that results are pertinent and show a viable representation of the flow trend. To ensure this, statistical analysis developed by Ronald Fisher in 1925, named the t-test, was used to show that the four cases performed are statistically significant from one another. As once proposed by Fisher, a significance of 5% was chosen to evaluate the cases with. Such a level of significance would be equivalent to stating that there is 1 chance in 20 that the hypothesis test is wrong, making it an acceptable level of significance [83]. Therefore, a p value below 5% would be desirable and would indicate that the case in question is indeed statistically significant. On the other hand, the h value simply indicates whether or not the case is statistically different from other cases studied. In other terms, an h value of 1 would indicate statistical difference while a value of 0 would indicate a lack of statistical difference.

As an initial screening of the cases, each was subjected to a t-test in order to ensure that it was first, statistically significant, and second, statistically different. The viscous energy dissipation recorded during the diastole period of each case was used as the chosen variable for this test. The results obtained showed that each of the four cases was indeed statistically significant as well as statistically different. All of the tabulated results are shown in Table 3.

Table 3: T-test results for individual cases

Severity of Regurgitation	h value	p value
Normal	1	1.3636×10^{-62}
Mild	1	8.4924×10^{-10}
Moderate	1	6.4213×10^{-5}
Severe	1	1.0911×10^{-25}

As a follow up test, the cases were compared to each other to make sure that the cases were different enough from each other and that the results were not repetitive. By doing so, one can be confident that each regurgitant severity is representative of its given classification. The results for the double t-test are tabulated in Table 4.

Table 4: T-test results for case comparison

Comparison between Severities of Regurgitation	h value	p value
Normal vs Mild	1	8.4924×10^{-10}
Normal vs Moderate	1	6.4213×10^{-5}
Normal vs Severe	1	1.0911×10^{-25}
Mild vs Moderate	1	0.0115
Mild vs Severe	1	3.0112×10^{-12}
Moderate vs Severe	1	1.0052×10^{-17}

3.10 Uncertainties

This experiment was performed using techniques and calculation methods that will limit errors and uncertainties. An example of such a technique is to have the hydraulic activation chamber also filled with the same water-glycerol mixture such that the distortion when using the PIV and camera setup is at a minimum. Furthermore, it goes without saying that there is an error percentage due to image quality, unfocused particle images and other such error sources. Additionally, in order to verify that measurements are accurately performed and recorded, pressure variation was analyzed to verify that the equipment was consistent in its performance. By comparing the five pressure cycles recorded for each case, less than 4% variation was found to have occurred, signifying that the equipment is indeed performing satisfactorily.

Chapter 4 - Results

The performed experiments have yielded the following results which will be discussed in the subsequent sections. After careful post-processing and analysis, velocity fields, angle of entry from the tricuspid valve, velocity profiles, circulation, viscous energy dissipation and proper orthogonal decomposition were the obtained results.

4.1 Velocity Fields

As a preliminary examination, the velocity field is observed for each case in order to have a notion of the flow in the right ventricle when regurgitation is present. Diastole, which is the filling phase of the ventricle, is a particularly interesting period which would show how the inflow jet would get affected by the regurgitant pulmonary jet.

4.1.1 Normal Case

The average flow of the diastolic period is a summary of several recorded instances and may reveal overall trends, however, it is potentially beneficial to look at a breakdown of the average in case there is a structure of interest that does not appear in the average. Following are a set of chosen instances during diastole as well as its beginning and end so that a clearer picture can be rendered and noteworthy structures can be observed. Figure 14 shows images of the normal case at the beginning of diastole ($t^*/T = 0.4$) as well as the beginning of systole ($t^*/T = 1$), which is the emptying phase**.** Figure 14 additionally shows three more images during diastole which are at approximately equal intervals of each other; $t^*/T = 0.55$, $t^*/T = 0.7$and $t^*/T = 0.85$.

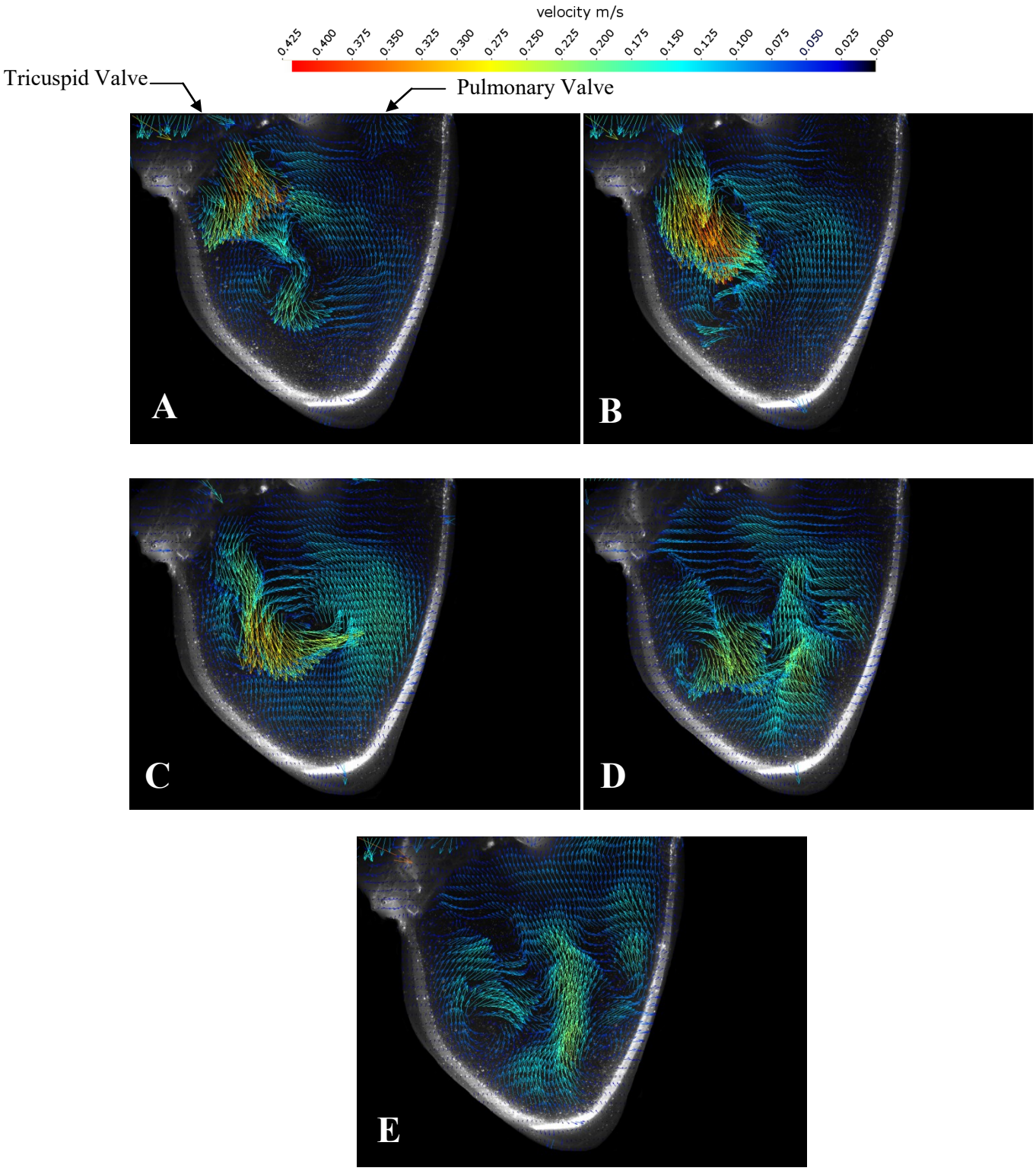

Figure 4.1: Velocity field in the right ventricle for the normal case at the beginning and end of diastole as well as three selected instants in between : (A) $t^*/T = 0.4$ (beginning of diastole), (B) $t^*/T = 0.55$, (C) $t^*/T = 0.7$, (D) $t^*/T = 0.85$, (E) $t^*/T = 1$ (beginning of systole).

From the above images, one can indeed agree that there does not seem to be any regurgitation occurring from the pulmonary valve and that the inflow into the ventricle is entering solely from the tricuspid valve. In Figure 14-A and B, the inflow jet appears to enter at a small angle with the left most endocardial wall and follows it down towards the apex, consistent with the time-averaged image of diastole previously seen. A small vortex ring can also be observed right underneath the tricuspid valve, consistent with the findings of ElBaz et al. [58]. Figure 14-C best depicts the counter-clockwise vortex that was faintly seen in Figure 15-A, further emphasizing the presence of this crucial structure. Figures 14-D and E seem to lack a bit of coherence when compared to the other images, however, it is clear that the overall fluid motion is of its exit towards the pulmonary valve, which is consistent with the end of diastole and the beginning of systole.

4.1.2 Mild Case

The mild case, which has an ROA/A of 0.012, shows some vastly different flow structure behaviors compared to the normal case, as can be seen in Figure 15.

In Figure 15-A, there is a clear flow incoming from the pulmonary valve, consistent with the fact that there is a regurgitation orifice present. An inflow, that seems to be larger in size, can also be seen entering the ventricle through the tricuspid valve although its velocity seems to be lower than that of the regurgitant. The inflow from the pulmonary valve can be observed flowing downwards along the rightmost endocardial wall and towards the apex, while the inflow from the tricuspid valve, as opposed to the normal case, is flowing across the ventricle and joins the regurgitant flow along the rightmost endocardial wall. This appears to create a large flow that is moving in clockwise fashion.

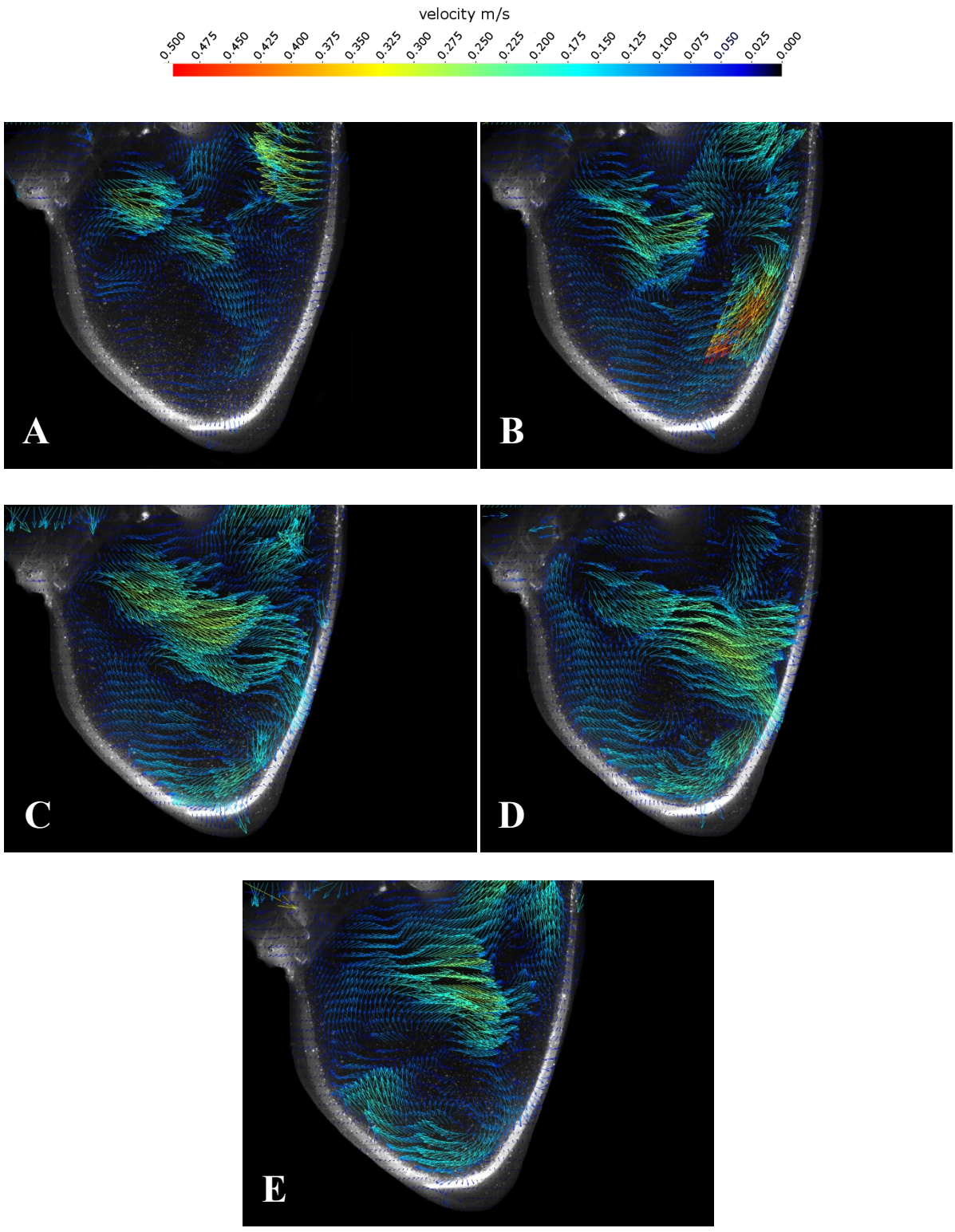

Figure 4.2: Velocity field in the right ventricle for the mild case at the beginning and end of diastole as well as three selected instants in between : (A) $t^*/T = 0.4$ (beginning of diastole), (B) $t^*/T = 0.55$, (C) $t^*/T = 0.7$, (D) $t^*/T = 0.85$, (E) $t^*/T = 1$ (beginning of systole).

This trend is particularly apparent in Figures 15-C and D. Once systole begins, the clockwise vortex can still be seen, as shown in Figure 15-E, however, some smaller vortices seem to have formed and some slight instability seems to be present.

4.1.3 Moderate Case

The moderate case which has a ROA/A of 0.063, shows a similar pattern to the mild case that was previously observed.

Concurrent with the enlargement of the regurgitant orifice, the inflow from the pulmonary valve seems to have a larger diameter than with that of the regurgitant in the mild case. The inflow from the tricuspid valve can be seen having a similar trajectory than the one in the mild case while its diameter seems to be smaller than the latter. Although there seems to be a bit more instability during filling, the main vortex that forms seems to be capable of maintaining its structure longer than in the mild case and is clear until the beginning of systole.

4.1.4 Severe Case

In this last case, one can clearly see that the only influx is coming from the pulmonary valve. With a ROA/A of 0.174, it seems that the flow created by the regurgitant prevents the tricuspid valve from opening, as seen in Figure 17-A. The same clockwise vortex that has been observed in the mild and moderate cases can also be seen in this case albeit seeming stronger and more stable. It appears that the reversed vortex takes up the entire ventricle and is visually the dominating structure throughout the diastole period.

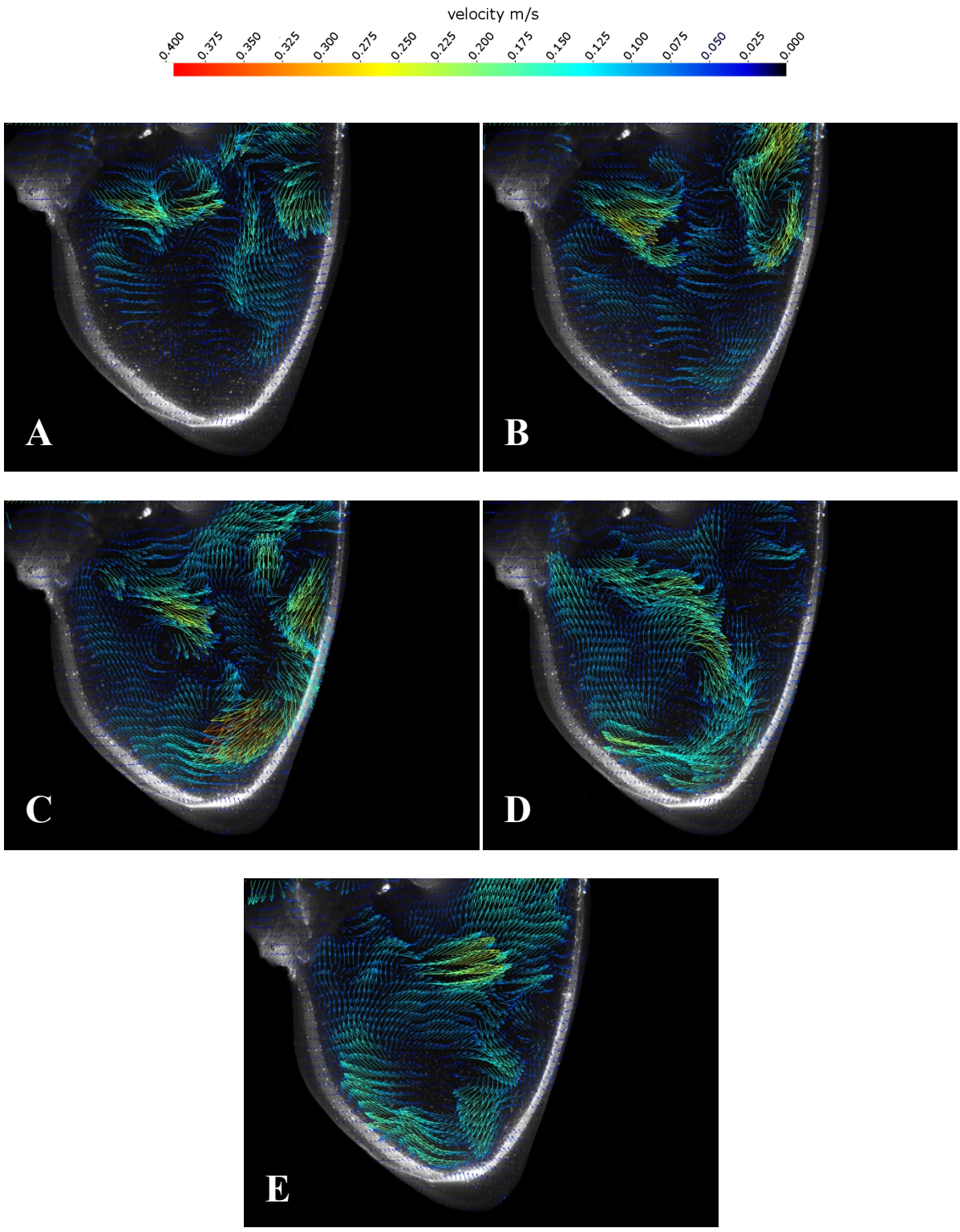

Figure 4.3: Velocity field in the right ventricle for the moderate case at the beginning and end of diastole as well as three selected instants in between : (A) $t^*/T = 0.4$ (beginning of diastole), (B) $t^*/T = 0.55$, (C) $t^*/T = 0.7$, (D) $t^*/T = 0.85$, (E) $t^*/T = 1$ (beginning of systole).

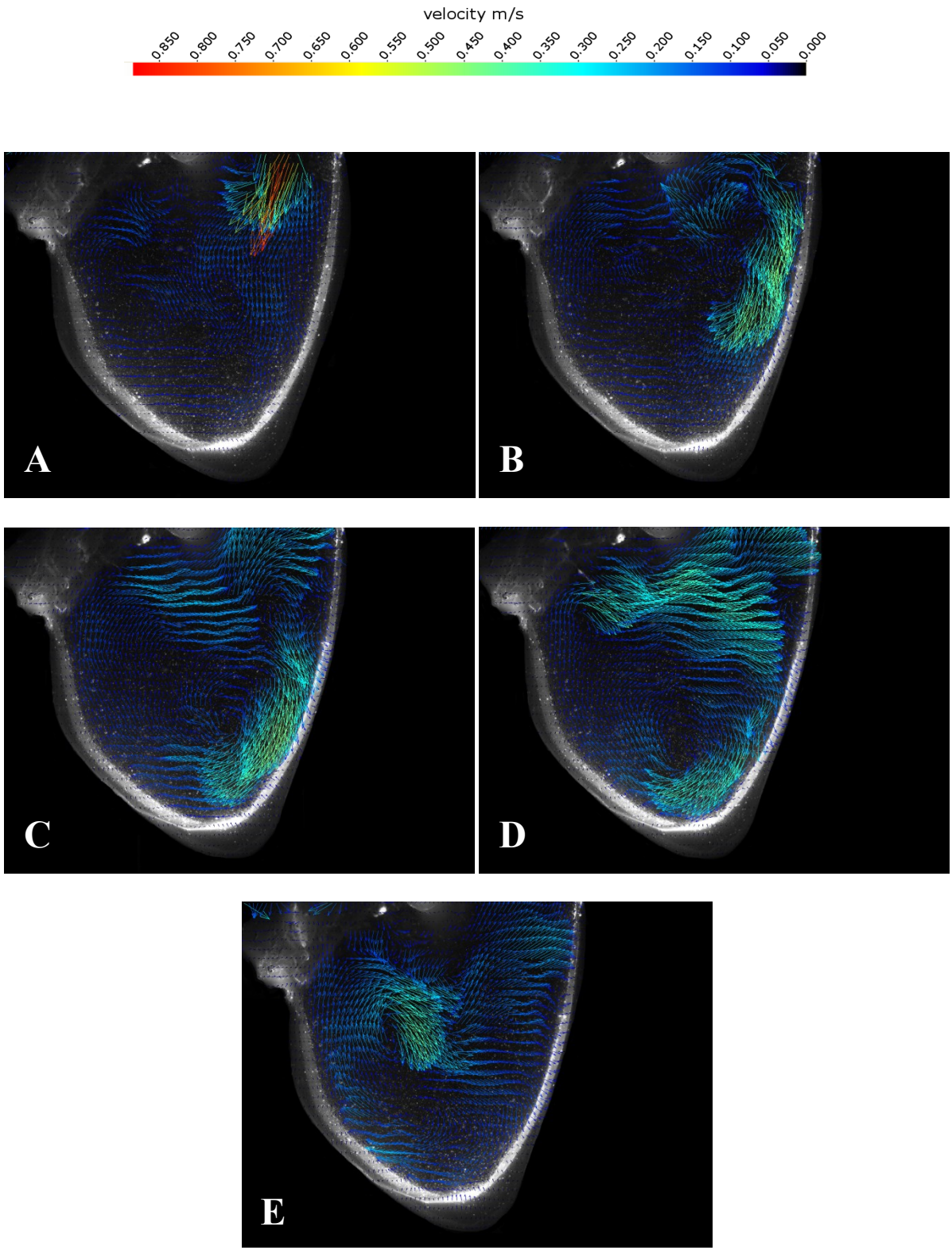

Figure 4.4: Velocity field in the right ventricle for the severe case at the beginning and end of diastole as well as three selected instants in between : (A) $t^*/T = 0.4$ (beginning of diastole), (B) $t^*/T = 0.55$, (C) $t^*/T = 0.7$, (D) $t^*/T = 0.85$, (E) $t^*/T = 1$ (beginning of systole).

Although there does not seem to be any inflow from the tricuspid valve at the beginning of diastole, Figure 17-D shows some flow from the tricuspid valve that is directly flowing in the same direction as the reversed vortex ring. One can also notice that this inflow is entering the ventricle at a much higher angle than in the normal case.

4.1.5 Average Velocity Fields

Figure 18 below shows the time-averaged velocity fields solely during diastole for all of the four cases. A color gradient is used to show the intensity of the flow vectors with red being at a higher velocity and blue being much lower in velocity. Additionally, white arrows have been added to show the overall direction of the inflow jet, irrespective of its intensity.

The normal case, which does not have any regurgitation present, shows a distinctive jet going down the left most lateral endocardial wall, as seen from a frontal view, towards the apex. Although this is but an average flow of diastole, one can also see the faint structure of a counter-clockwise vortex. This is corroborated by works done by others such as Pedrizzetti [56] and Pasipoularides [57], who claim that such a structure is vital to the proper functioning of the ventricle.

Once regurgitation is introduced, as in the mild case, the trajectory of the inflow that was observed in the normal case slightly changes. One can observe that the inflow, in this case, is shifted slightly upwards and crosses the ventricle towards the opposite rightmost lateral endocardial wall on which it then flows downwards towards the apex. Because of this change in orientation, one can notice that the counter-clockwise vortex that was previously observed in the normal case, now has reversed and became a clockwise vortex.

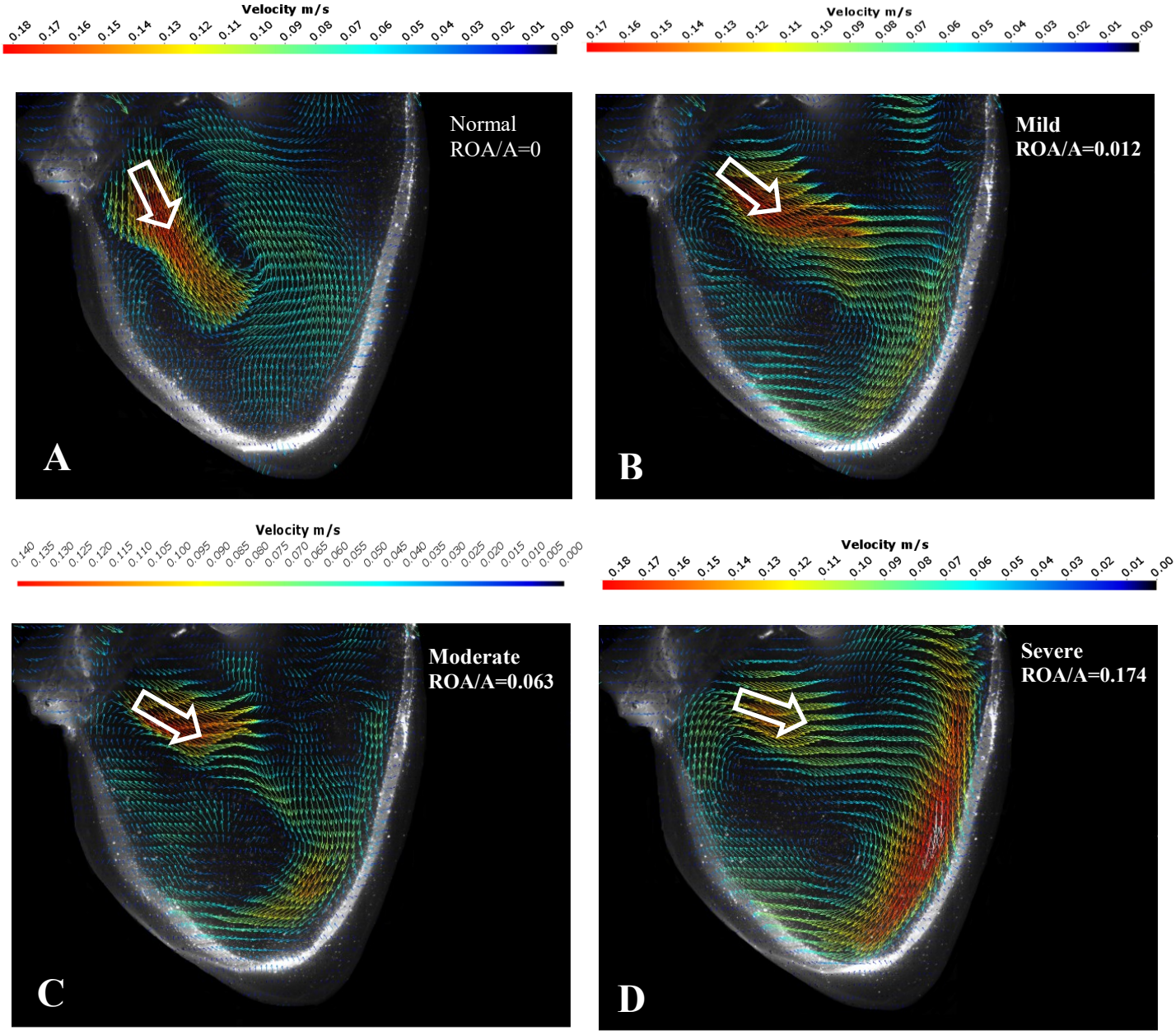

Figure 4.5: Time-averaged velocity fields during diastole for: (A) normal case, (B) mild pulmonary regurgitation, (C) moderate pulmonary regurgitation, and (D) severe pulmonary regurgitation.

The moderate regurgitation case shows a similar pattern as the mild one with a comparable angle for the inflow jet and a clockwise vortex. However, it would be interesting to note that the

increasing amount of regurgitation seems to slightly disrupt the jet crossing the ventricle and heading towards the right most lateral endocardial wall.

Lastly, the severe case depicts an even larger angle for the inflow jet, however, this jet is quite significantly diminished compared to the previous cases. Furthermore, one can clearly see that the vast majority of inflow into the ventricle is from the pulmonary valve regurgitant which simply flows down the right most lateral endocardial wall and towards the apex, forming an even more apparent clockwise vortex.

4.2 Angle of Entry from the Tricuspid Valve

With the flow changing drastically once regurgitation is introduced, one must wonder what is the effect of such changes on the inflow from the tricuspid valve. In answer to this, the angle of entry from the tricuspid valve was examined and the average inflow angle is displayed in Figure 19 below.

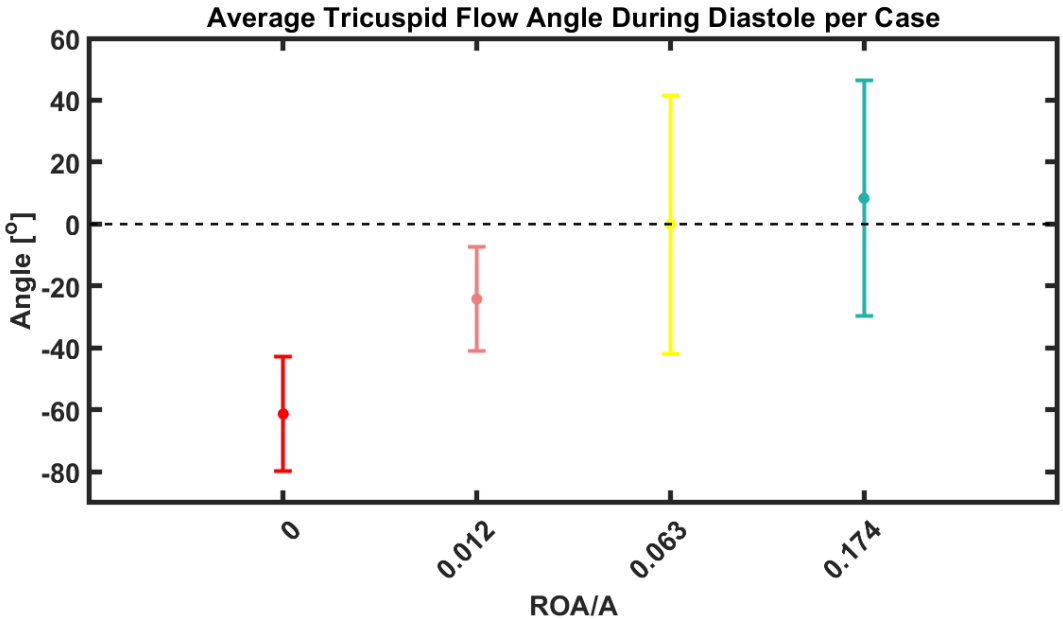

Figure 4.6: Average angle of tricuspid valve inflow for all cases during diastole

Based on these results, it seems that there is a correlation between the increase in inflow angle from the tricuspid valve and the severity of the regurgitation. The graph clearly portrays that as the amount of regurgitant increases from the pulmonary valve, the angle of tricuspid inflow is no longer negative and flowing downwards towards the apex but instead flowing at a more positive angle and therefore crossing the ventricle towards the opposing endocardial wall.

4.3 Velocity Profiles

Velocity profiles can aid in the visualization of the flow direction either at an instant or as an average during a time period. Here, the velocity profile is shown for all four cases as an average during diastole. The profiles were also normalized by using the maximum velocity observed during this time period for each case respectively. Furthermore, all velocity profiles were taken at the same location in the ventricle which is right in the center of it, as depicted on the pictograms below.

Finally, each pictogram depicts the inflow from the tricuspid valve as well as from the pulmonary valve, if present, with black arrows indicating the severity of the inflow. A red arrow is also present in each pictogram, representing the overall flow direction in the ventricle. The velocity profile in the normal case can first be observed below in Figure 20.

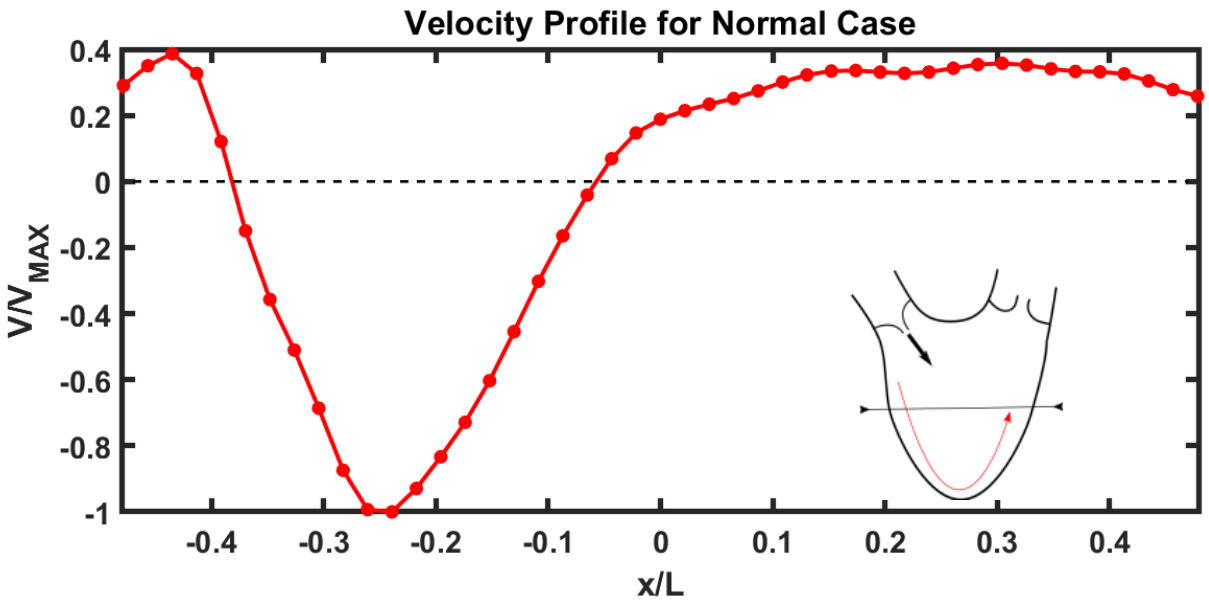

Figure 4.7: Velocity profile during diastole for the normal case

As previously seen in the velocity fields images, the velocity profile for the normal case shows how a large flow is moving downwards the left most lateral endocardial wall and towards the apex of the ventricle. This is consistent with the previous observation of a counter-clockwise vortex during diastole for the normal case.

Once a slight regurgitant is introduced via the pulmonary valve, as seen in Figure 21, the velocity profile drastically changes compared to the normal case. The downwards flow towards the apex by the left most lateral endocardial wall is no longer observed and instead, a seemingly alternating upwards and downwards flow throughout the length of the ventricle as well as a small downwards flow next to the rightmost lateral endocardial wall.

Figure 22 portrays the velocity field for the moderate case and one can observe that the flow is slightly more hectic than for the mild case. Although there seems to be some slight instability in the flow, a downwards flow near the rightmost lateral endocardial wall is still present.

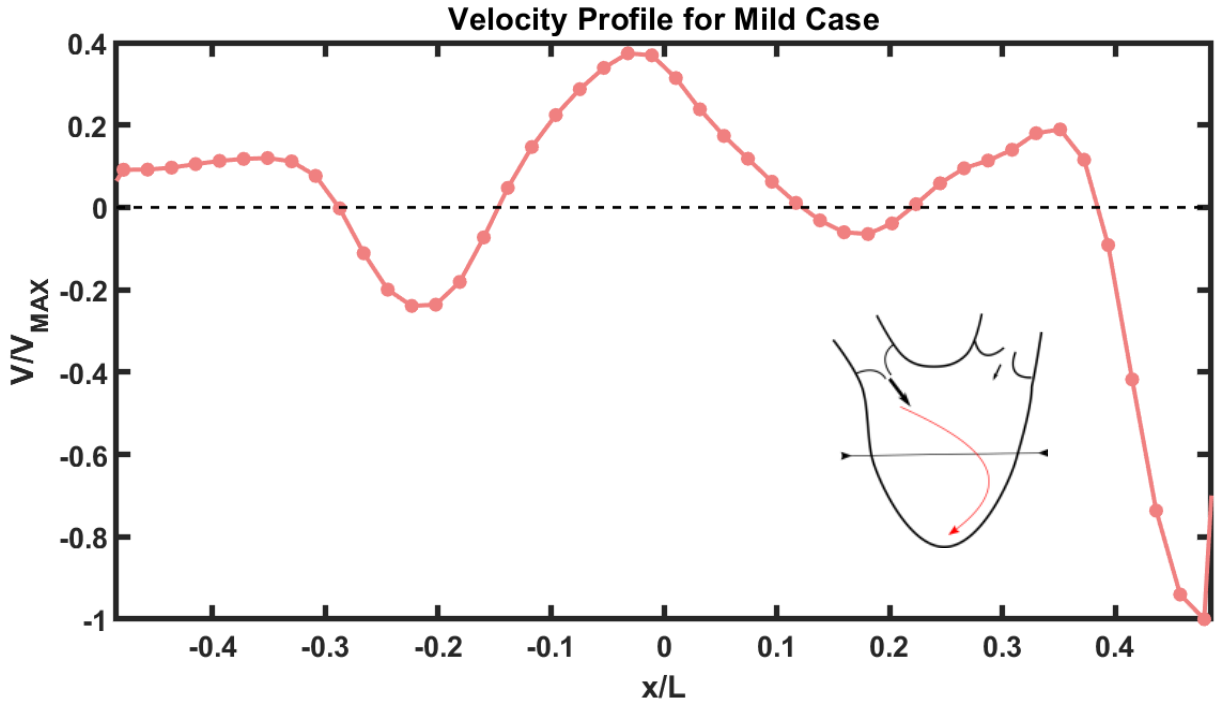

Figure 4.8: Velocity profile during diastole for the mild case

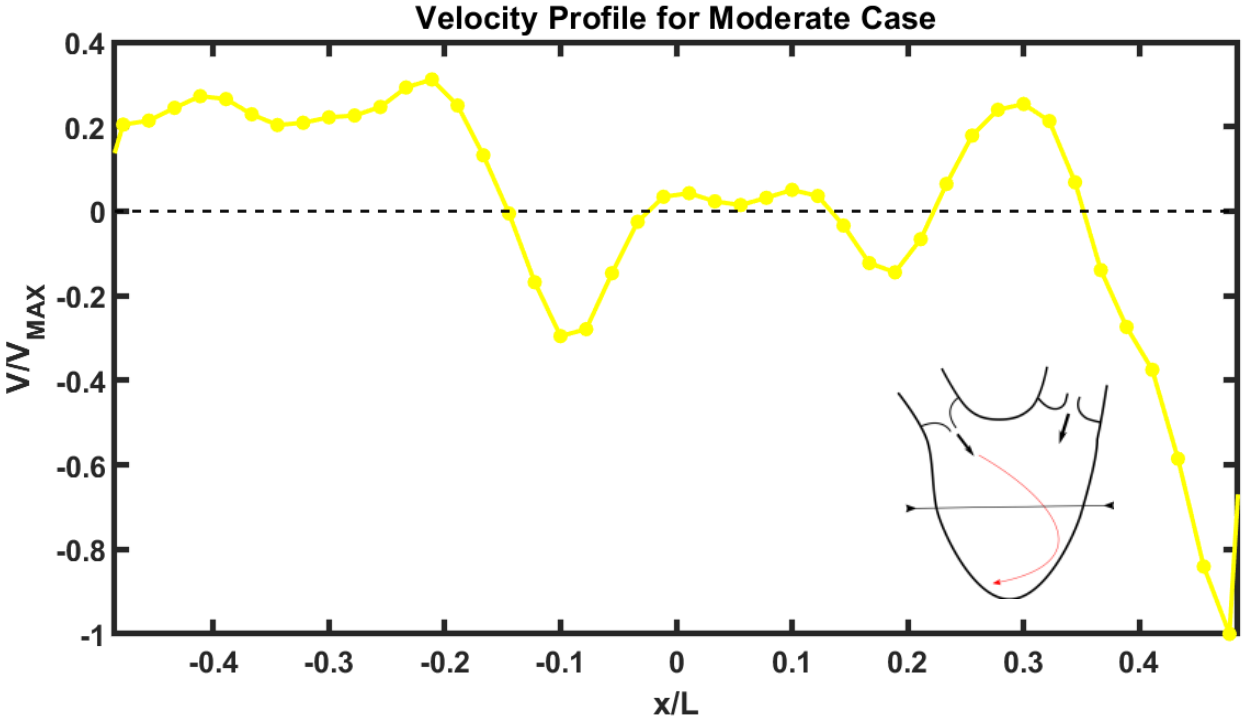

Figure 4.9: Velocity profile during diastole for the moderate case

Lastly, the velocity profile for the severe case, as seen in Figure 23, portrays the flow to be more stable and quite similar to the normal case albeit it in a reversed fashion. In fact, one can describe the velocity profile for the severe case as being almost the mirror image of the one for the normal case, with the downwards flow being next to the rightmost lateral endocardial wall instead of the leftmost one. Once again, this flow pattern can also be seen in the velocity field images when the bulk of the flow is entering through the pulmonary valve and circulates in a clockwise fashion.

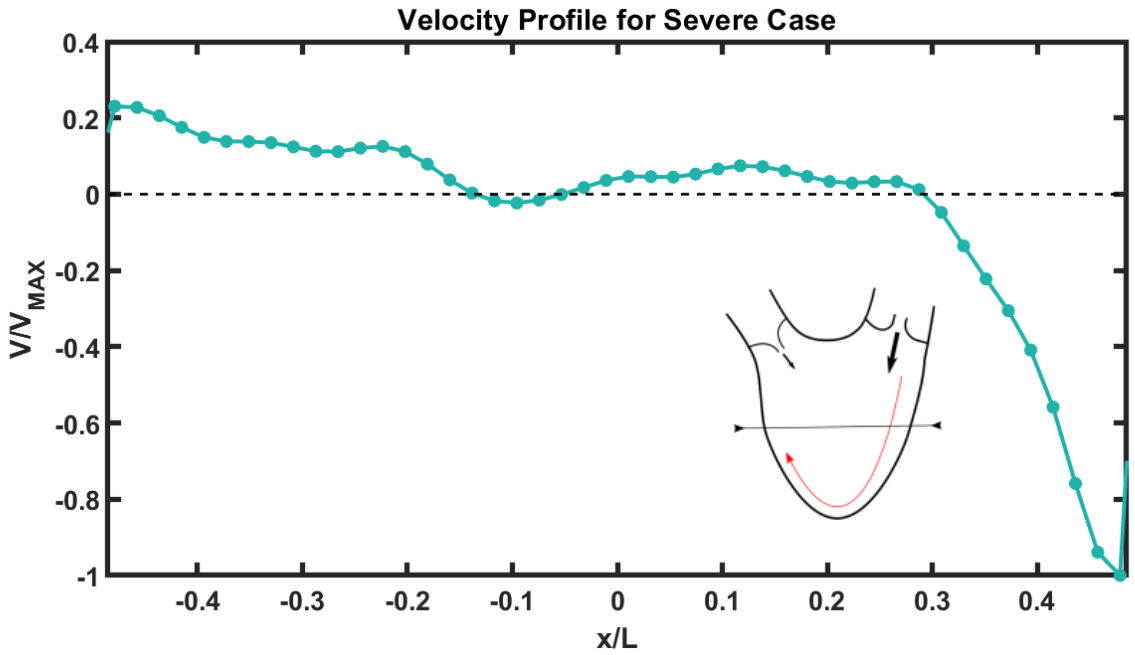

Figure 4.10: Velocity profile during diastole for the severe case

4.4 Circulation

As mentioned previously, vortices are crucial for the proper functioning of both the right and left ventricles. Naturally the presence and state of the vortices give an indication regarding the functioning of the ventricle and whether it is compromised or not. Aside from the velocity fields and viscous energy dissipation, circulation is another parameter useful in qualifying the flow in the ventricle with the counter-clockwise flow having positive circulation while the

clockwise flow is referred to as having negative circulation. Figure 24 depicts the circulation present in the right ventricle for all of the cases during diastole.

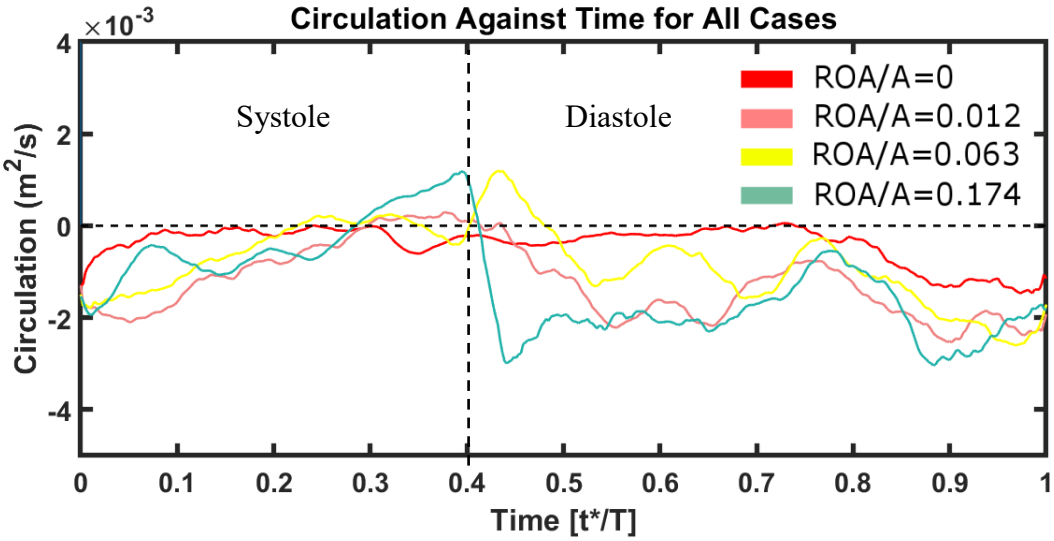

Figure 4.11: Circulation against time for all four cases during diastole

.

Although all of the cases seem to have negative circulation, the normal case, which is the reference, is very close to the zero reference line indicating that amount of positive and negative circulation in the ventricle are similar and cancel each other out. This can also be due to the vortex ring that be observed in the normal case velocity field. As the severity of regurgitation increases, so does the level of negativity of the circulation with the severe case having the largest amount of negative circulation. Although both the mild and moderate cases have overall negative levels of circulation, the above graph depicts the moderate case having similar levels to the normal case while the mild case has slightly higher levels of negative circulation. One can also observe a negative run down in the three cases with regurgitation between the 0.4 and 0.55 time stamps. These dips are most likely due to the inflow of the regurgitant since the severe case has by far the largest drop in circulation negativity.

Another method of visualizing the amount of circulation for every case is shown below in Figure 25 where the total amount of circulation for each case is depicted.

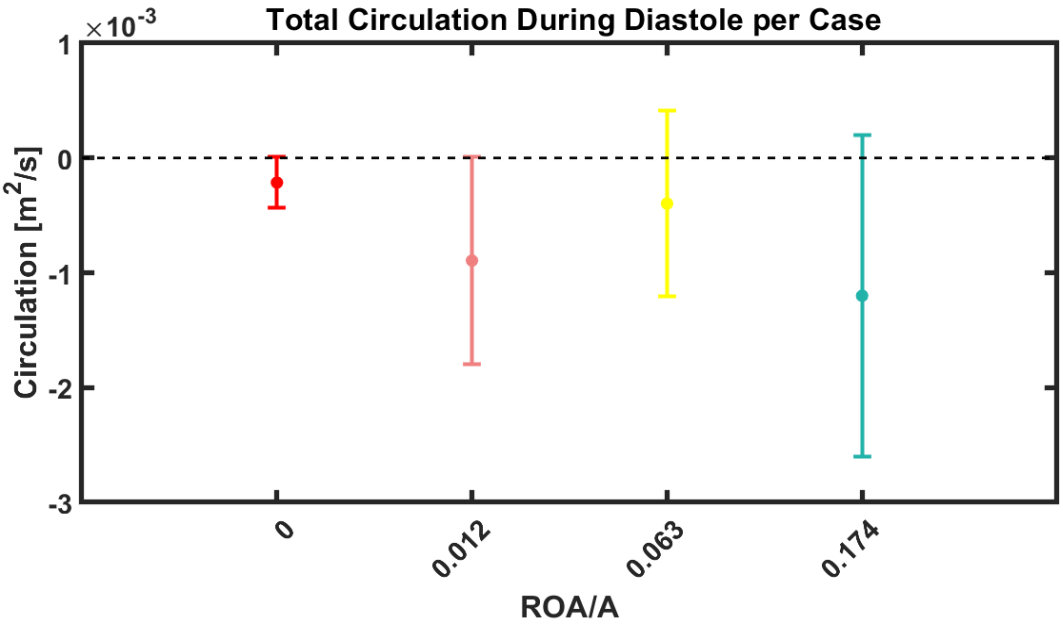

Figure 4.12: Total amount of circulation for each case

Figure 25 depicts a similar narrative as the previous Figure 24 where all of the cases seem to have an overall negative circulation, with the normal case being very close to the zero reference line. All of the other cases with regurgitation present have an increasingly negative circulation, the severe case being the one with the largest level of negative circulation. As opposed to in Figure 24, one can clearly observe that the moderate case is the closest case to the normal case while the mild severity has a higher level of negative circulation.

4.5 Viscous Energy Dissipation

Viscous energy dissipation is, in this case, primarily due to the viscous friction in the flow. Therefore, it would provide one with an essential tool in analysing and comprehending the flow present in the right ventricle.

As previously mentioned, a 2D cartesian coordinate system was used in order to apply the energy loss equation.

The computed results are shown below solely for the diastole period, which is of interest. Figure 26 below displays the energy loss with respect to time for all of the four cases.

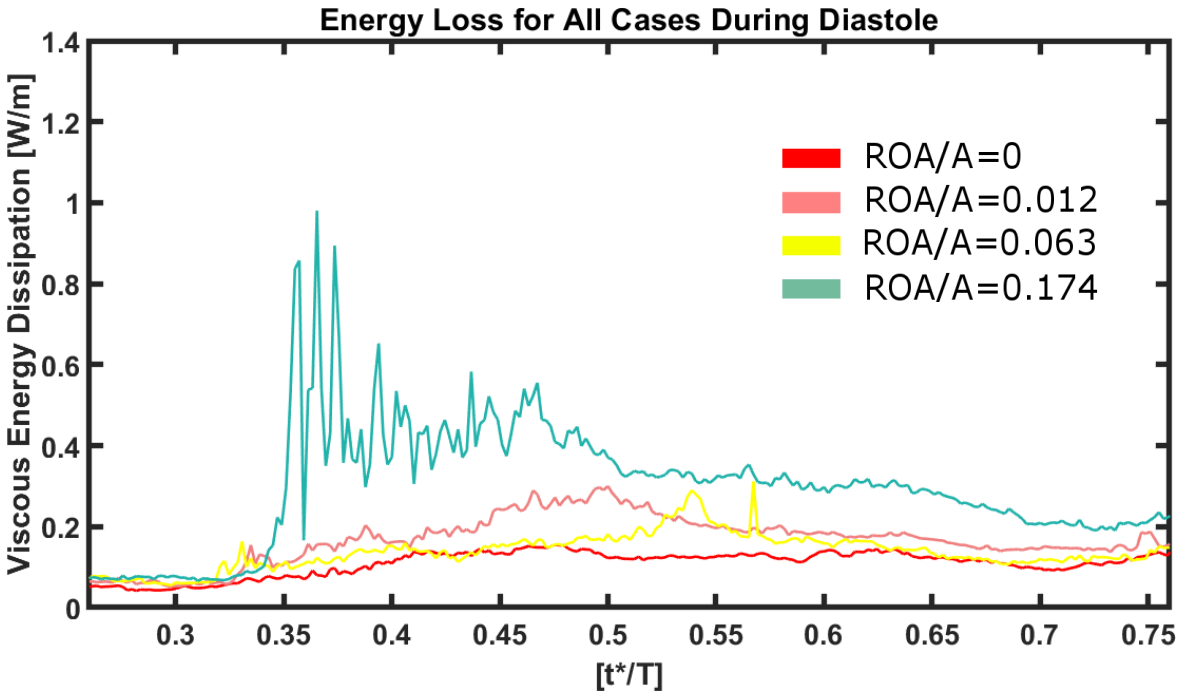

Figure 4.13: Viscous energy dissipation over time for all four cases

As seen from the above figure, the severe case seems to have the highest amount of energy loss throughtout diastole compared to all of the other three cases, while the norml has the lowest. This would appear to be correct since the severe case has the largest regurgitant orifice while the normal case lacks one. On the other hand, the mild and moderate cases appear to be comparable, however, the mild case exhibits certain periods where its overall energy loss exceeds that of the moderate case, making the moderate case more comparable to the normal case. There are only three minor instances where the energy dissipation displayed by the moderate case outdoes that of the mild case.

As another method of visualizing the energy loss in every case, the time average amount of energy during diastole can be displayed alongside the standard deviation. Figure 27 below portrays just that, offering a simple visualization of the total energy loss for each case.

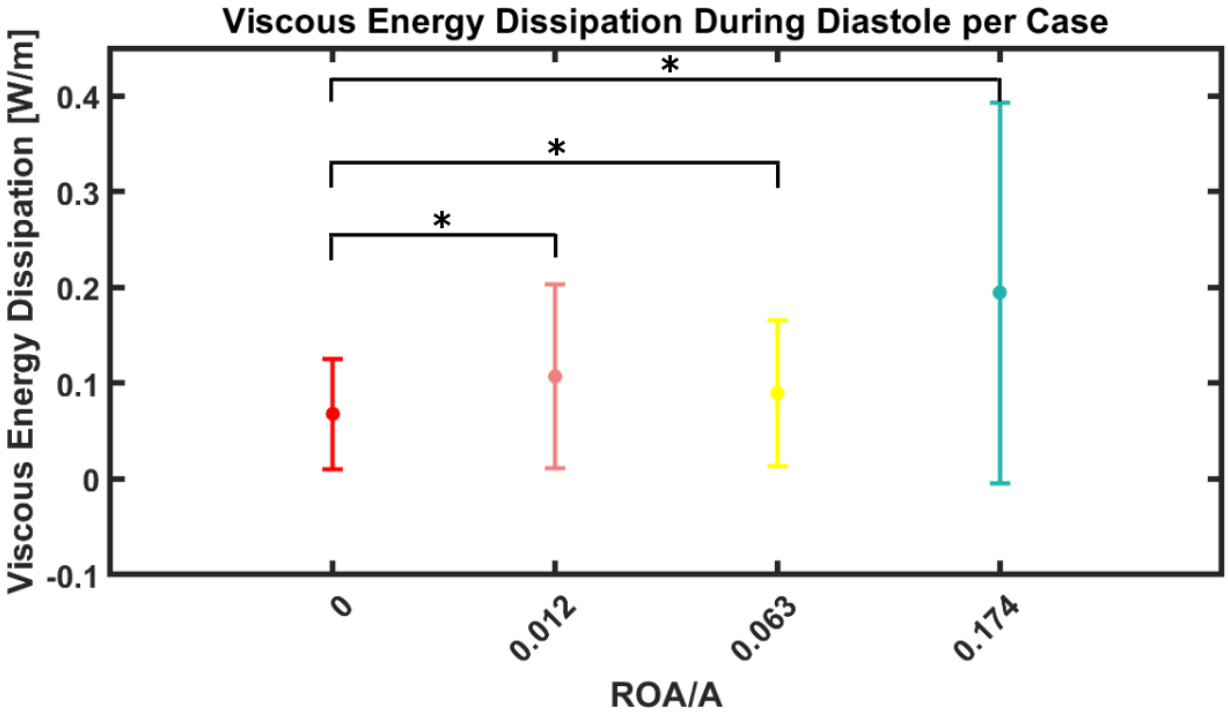

Figure 4.14: Average energy loss with standard deviation for all four cases during diastole (* = $p<0.05$)

Similar to the observations made on Figure 26, Figure 27 shows how the severe case has the largest total energy loss during diastole while the normal case has the lowest. Additionally, the mild and moderate cases are yet again comparable, however, the mild case seems to have a slightly elevated average amount of viscous energy dissipation during diastole compared to the moderate case.

4.6 Proper Orthogonal Decomposition

If proper orthogonal decomposition were to be explained in a simplified manner, one would say that it aims to break down a flow into the structures containing the highest kinetic energy and therefore, in theory, into the structures that contribute the most to the overall flow. These structures are shown as screenshots and are ranked based on the amount of kinetic energy contained within them and are called modes. The first mode obtained after computations is sometimes referred to as the average mode which represents the likeliest structure to be observed in the flow. It is comprised of the second mode and all of the following ones computed. In the case of this research, the first two modes are reported for each of the four cases during diastole. Below, in Figure 28, are the first two proper orthogonal decomposition modes for each of the four cases alongside their respective average velocity field for diastole.

Naturally, since the first mode and average velocity fields are the same, then it is safe to say that structures observed in either of those images correspond to a large portion of the kinetic energy present during diastole. It also means that these structures are dominant during diastole. More precisely, the normal case is defined by the inflow entering solely through the tricuspid valve as well as a vortex ring comprised of a large counter-clockwise flowing vortex.

Both the mild and moderate cases are defined by a reversed vortex flowing in a clockwise manner. The same can also be said to describe the severe case albeit the velocities observed in this case are a lot higher than for the mild and moderate cases.

In accordance to all of the explanations previously given, each mode is ranked based on the amount of kinetic energy it represents. That being said, the overall fluid flow that is under examination can theoretically be reconstructed at, for instance, a 98% confidence with a certain number of modes. The more energy the modes represent, the lower the number of modes

necessary to reconstruct the flow. Figure 29 illustrates the cumulative fraction of the total modal energy for the first thirty-five modes for all four cases. Simply stated, it represents how many modes are necessary to reconstruct each severity case with a confidence of 98%.

As observed in the above figure, the normal case is the one that requires the least amount of modes to attempt to reconstruct the flow at a 98% confidence. This signifies that more energy is contained in a fewer number of modes and therefore making it likely that they contain coherent structures. Of course, more post processing of the data is required in order to ensure this. The following three cases with regurgitation seem to require more modes as the severity of the regurgitation increases. For the mild case, it seems that about twenty modes are required which is not much less than the moderate case which appears to require between twenty-three modes. In contrast, the severe case requires approximately thirty-four modes in order to reconstruct the flow, making it the highest requirement of all the cases. These numbers are tabulated in Table 5.

Furthermore, one can note that the global entropy of the cases, portrayed in Table 5, show that as the regurgitation increases, so does entropy. However, it is interesting to note that the entropy for the severe case is actually lower than the one in the moderate case. Once again, this might speak to the probable increase in stability in the severe case.

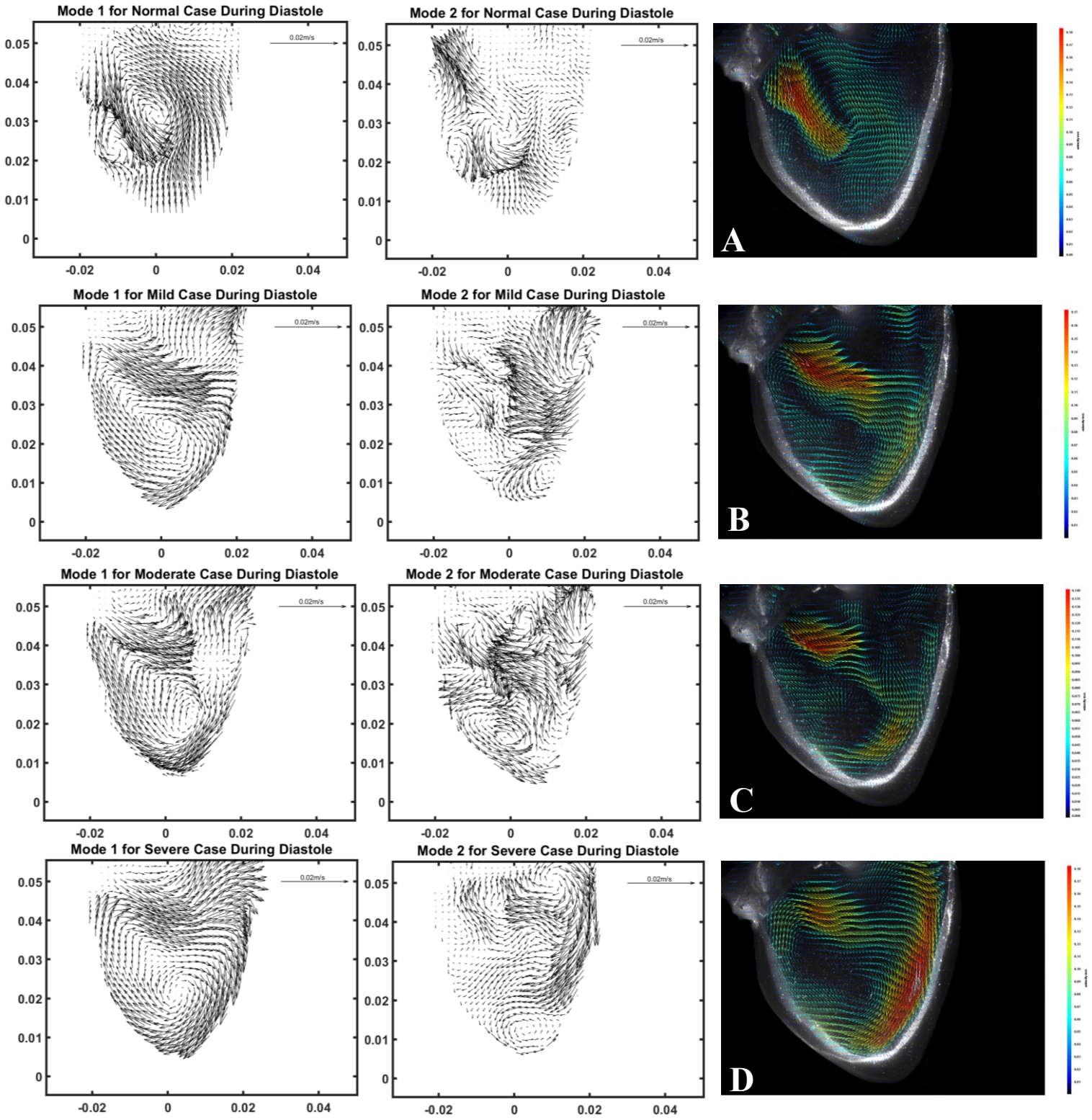

Figure 4.15: First proper orthogonal decomposition mode during diastole alongside the average velocity during diastole for (A) the normal case, (B) the mild case, (C) the moderate case, and (D) the severe case.

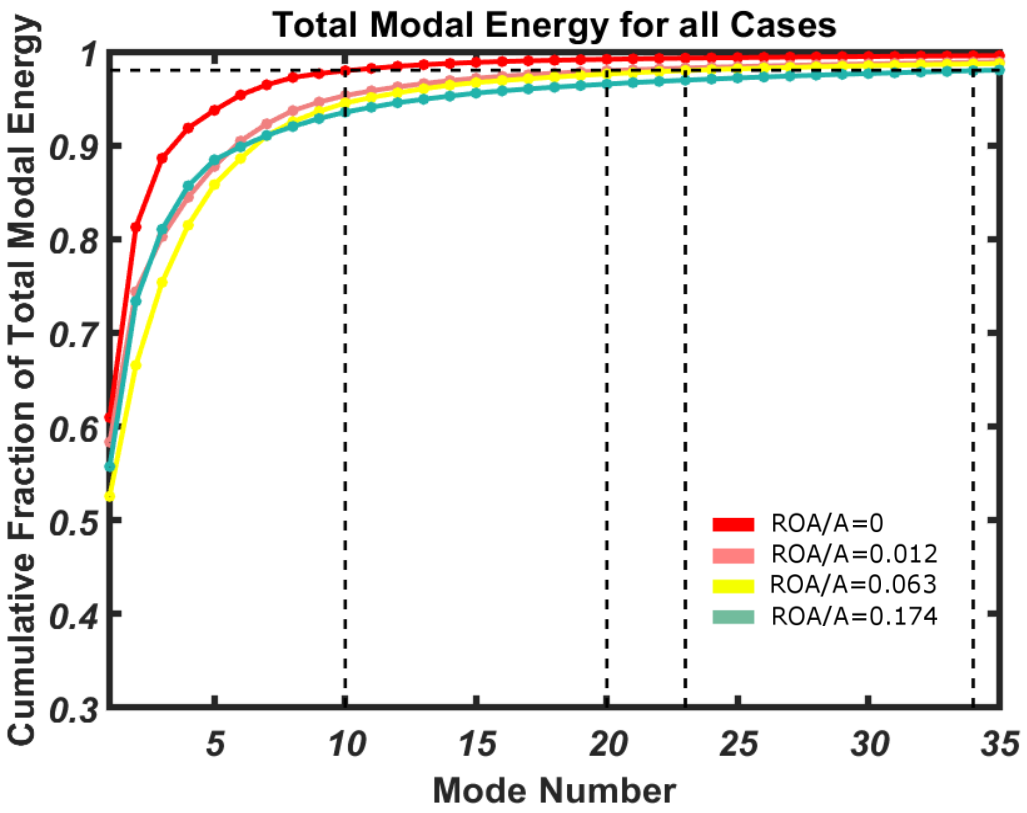

Figure 4.16: Total modal energy for all of the four cases

.

Table 5: Required number of POD modes and global entropy for each experimental case

Case Severity	ROA/A	Number of POD Modes	Global Entropy H
Normal	0.000	10	0.2722
Mild	0.012	20	0.3254
Moderate	0.063	23	0.3662
Severe	0.174	34	0.3422

To further emphasize the number of modes required to reconstruct the flow in each of the four cases, Table 6 tabulates the kinetic energy percentage present in the first three modes of each case. As expected, the first mode in the normal case contains the highest amount of energy with

61%. In comparison, the severe case has its first mode with the lowest amount of kinetic energy of 56% and more modes are required to reconstruct the flow. A similar trend can be seen with the second and third modes, although some exceptions to the trend might appear, such as the second mode in the severe case having a higher percentage than the one in the moderate case. This might speak to the hypothesis that the reversed flow in the severe case is more stable than the ones observed in the mild and moderate cases.

Table 6: First three modes for all cases and their kinetic energy percentages

Case	Mode	Kinetic Energy Percentage
Normal	1	61%
	2	20%
	3	7%
Mild	1	58%
	2	16%
	3	6%
Moderate	1	53%
	2	14%
	3	9%
Severe	1	56%
	2	18%
	3	8%

Chapter 5 - Discussion

Due to the lack of understanding of the fluid dynamics in the right heart, this novel experiment aims to gain a deeper insight into the fluid flow in the right ventricle when pulmonary valve regurgitation is present where physical simulations must be carefully performed so as the adequately reproduce the fluid flow in the ventricle. As mentioned previously, in reason of a lack of guidelines for the categorization of pulmonary valve regurgitation, the arbitrarily chosen orifice areas and regurgitation severities are simply to show the progression of dynamic flows until a better categorization is present in literature. The different severities of regurgitation are to give a more fuller and complete understanding of the flow trends that occur in the right ventricle. Several variables, such as velocity, viscous energy dissipation and circulation, were calculated for all cases in order to observe their trends and change across the various cases. Although each variable can be calculated in such a way that several units are possible, the dimensions chosen in this experiment are for the ease of understanding and usefulness towards clinicians.

When analysing these four cases, the diastolic period was chosen as the most pertinent time to observe. By looking at the filling period, one can examine the influence the regurgitant has on the normal flow structures present in the right ventricle. As a result, the average velocity field during the filling period was computed. At a first glance, the average velocity field for the normal case shows a substantial inflow from the tricuspid valve and nothing from the pulmonary valve, as is expected. Also, the overall flow motion can be said to resemble a counter-clockwise vortex with a vortex ring below the tricuspid valve. Based on published literature from Pasipoularides et al. [57] and ElBaz et al. [58], the proper functioning of a right ventricle does

indeed require the presence of a counter-clockwise vortex. Therefore, this is a indication that the normal case does indeed simulate the expected flow structures that would occur *in vivo* and that the overall setup of the experiment should yield useful and pertinent results. The angle of the tricuspid inflow can also be commented on. The inflow from the tricuspid valve for the normal case is seen entering the ventricle downwards and at an acute angle with the vertical axis. It seems highly probable that this particular angle aids in the direction of the counter-clockwise vortex. Such a hypothesis could be supported by the fact that both the flow structures and inflow angle from the tricuspid valve change drastically, in such a way that a relationship could exist, as the severity of the regurgitation increases throughout the cases. To better illustrate this hypothesis, a closer look at the other three cases can be taken. Once a mild regurgitant of 0.012 ROA/A of the valve orifice is introduced, the flow dynamics can already be observed to considerably change. The average velocity field for the diastolic period of this case shows how instead of the overall flow being a counter-clockwise vortex, it has now reversed and become a clockwise vortex. In addition to this, the angle of entry has shifted upwards, meaning that it has increased and is less of an acute angle. It is difficult to say whether this is a by-product of the angle change or not, but the trajectory of the inflow is no longer along the endocardial wall below the tricuspid valve, but rather, it crosses the right ventricle cavity until it reaches the opposing endocardial wall where it then flows downwards towards the apex. This change in flow direction could be a major contributor to the reversal of the overall vortex that forms during diastole. This same pattern can also be seen for the moderate case where a regurgitant of 0.063 ROA/A of the valve orifice is introduced. Although, once again the entry angle is increasing, the flow trajectory of crossing the ventricle cavity and the clockwise vortex are still observed but with the presence of what appears to be flow instability. The last case, which is the severe one

with a regurgitant of 0.174 ROA/A, shows the overall same pattern as in the mild and moderate cases with the exception that the inflow is quite significant entering through the pulmonary valve. This inflow is seen flowing down the endocardial wall right below the pulmonary valve and down towards the apex. Once again, although it is unclear if this flow is the cause of the vortex reversal, it most likely makes a significant contribution to the stability of said vortex. A last remark regarding this case is the angle of entry of the slight inflow from the tricuspid valve. Although the majority of the inflow is entering through the pulmonary valve, the slight inflow from the tricuspid valve can be observed entering at an even larger angle than in the normal case. The pattern deduced from these cases is that the larger the regurgitant is, the larger the angle of entry from the tricuspid valve until this inflow is virtually perpendicular to the vertical axis. A hypothesis regarding this phenomenon would be that the inflow from the regurgitation is strong enough to disturb the natural flow in the right ventricle and instead cause the flow to reverse. This reversal could potentially cause the tricuspid inflow to follow this new induced flow and therefore cross the ventricle cavity. As the regurgitant increases in strength, so does the pull of this new flow, therefore increasing the angle of entry from the tricuspid valve. As one may point out, these observations are done on an average velocity field and may potentially not illustrate everything that is occurring throughout these flows. Therefore, a breakdown of diastole by way of observation of the velocity fields at several instances might yield further insight and potentially reinforce the claims and observations previously made. In this regard, five instant velocity fields were looked at for each case including the start of diastole ($t^*/T = 0.4$), $t^*/T = 0.55$, $t^*/T = 0.7$, $t^*/T = 0.85$, and at the beginning of systole ($t^*/T = 1$). These velocity fields for the normal case are shown as part of Figure 14. Although a clear inflow through the tricuspid valve can be seen in Figure 14-A and 14-B, instability seems to be present overall. However, the

counter-clockwise vortex can indeed be observed in Figure 14-C, making our previous observations regarding the presence of the vortex viable. The acute angle of the inflow can also be observed in Figure 14-A and 14-B and no inflow can be seen from the pulmonary valve, making one even more confident that this case does indeed accurately portray a normal/healthy case. In regards to the observed turbulence, the apparent lack of coherence could be due to the fact that the structures are not visible in their entirety since they are not viewed three dimensionally. Seeing only a "slice" of a structure provides only a glimpse of the actual flow produced in the ventricle, therefore, the lack of coherence that is viewed could simply be a false impression since one cannot see the "whole picture". This hypothesis could hold true for all of the cases although stronger flows such as in the severe case seem to have less instability present. The mild case seems to still exhibit some instability, however, a vortex with a clockwise motion can be seen in Figure 15-B through E, making one deduce that this a dominant structure that is present for the majority of diastole. This is validated by the fact that the average velocity field for the mild case also shows a clockwise vortex. The mild regurgitation is also justified for this case because two inflow jets, from the tricuspid valve as well as from the pulmonary valve, can be observed in Figure 15-A. And lastly, the increase in inflow angle from the tricuspid valve can be seen throughout most of the velocity field images but especially in Figure 15-A. Similarly, the velocity field images for diastole for the moderate case show a comparable trend to the mild case where a clockwise vortex can be seen in Figure 16-C through E. Figure 16-A and B mainly depict the two inflows entering the ventricle from the tricuspid and pulmonary valves. In comparison to the mild case, the regurgitant in the moderate case appears to have a larger diameter than for the mild case, as is expected. Furthermore, the angle of inflow for the tricuspid valve seems to also increase in comparison to the mild case. What is interesting is that one might

be inclined to claim that the moderate case seems to exhibit slightly more instability than in the mild case which would be counterintuitive since one would be inclined to say that the stronger the flow, the less instability there should be. It is plausible that due to the small orifice of regurgitation present during the mild regurgitation case as well as a higher pressure in the pulmonary artery, the velocity of the inflow might be higher than for the moderate case which has a larger orifice diameter. At higher velocities, the flow might be dominated by the jet, allowing for the vortex to form more easily and with less instability. Since the regurgitant orifice is larger in the moderate case, the two inflow jets are becoming more comparable and might interact with each other more due to their similar velocities, causing an increase in instability. Additionally, since the regurgitant orifice is larger than in the mild case, then the pressure observed in the pulmonary artery isn't as elevated during diastole, hence no longer creating a high velocity jet that governs the flow in the ventricle. The last case, which is with severe regurgitation, illustrates an extreme scenario where the onset of diastole is characterized by a single inflow from the pulmonary valve as is seen in Figure 17-A. In fact, none of the velocity field images show a clear inflow from the tricuspid valve, indicating that the pressure in the ventricle during this case is high enough to either prevent the tricuspid valve from opening or only allowing it to open slightly, in which case the chosen velocity fields do not clearly show its inflow. The high-velocity jet from the pulmonary valve directly descends the endocardial wall and creates a much stronger clockwise vortex ring than in any other case.

To support the claim that, through visual deduction, the angle of flow entry through the tricuspid does indeed increase, Figure 19 unequivocally illustrates the average angle of inflow from the tricuspid valve increasing alongside the increase in regurgitation. Both the normal and mild case have negative inflow angles, meaning that these jets are moving downwards with respect to the

vertical axis. In contrast, the severe case exhibits a positive angle while the moderate case has an inflow angle very close to zero, meaning that it is flowing almost perfectly horizontally. The positive angle of entry during the severe could be due to the strong inflow from the pulmonary valve, which likely pulls the smaller inflow towards it.

Visual deduction of the flow patterns present based on velocity fields is not enough to certify that these structures are indeed present and not simply seen due to the choice of presented velocity fields. A method of achieving this is by analyzing the average velocity profile at a chosen location in the ventricle and seeing what is the overall motion of the fluid inside of the ventricle. For these four cases, the velocity profile was observed at the center of the ventricle along the horizontal axis. It is presumed that such a location would impart the most useful information since it should capture any large fluid motions. Figures 20, 21, 22, and 23 all corroborate the findings previously expressed when looking at the average velocity fields during diastole. The average velocity profile for the normal case shows a sharp downwards jet towards the apex, right below the tricuspid valve. This is in accordance with all of the velocity fields observed for this case. The velocity profile also depicts a slightly positive, in other words upwards, motion throughout the rest of the ventricle. Added to the downwards motion, presumable of the inflow, the overall motion of the fluid seems to be of a counter-clockwise vortex ring. Once the mild regurgitation is introduced, the velocity profile drastically changes and the downwards jet is seen to occur near the opposing endocardial wall with a slightly larger magnitude than in the normal case. The rest of the ventricle shows signs of instability since both positive and negative peaks can be observed. However, the area before reaching the endocardial wall below the tricuspid valve has a positive flow, leading one to believe that there is a clockwise motion occurring in the ventricle. The same pattern can be seen for the moderate case where a downwards peak is visible

near the endocardial wall below the pulmonary valve albeit not being as strong as the one in the mild case. This could be grounds to reinforce the theory that the regurgitant orifice in the mild case is small enough to create a high velocity flow downwards towards the apex. In contrast, the orifice in the moderate case could be large enough to interfere with the inflow from the tricuspid valve, hindering the potential high velocity of the regurgitant. Nonetheless, a positive flow can still be observed on the opposite side of the ventricle, once again supporting the notion of a clockwise vortex as is illustrated in the velocity fields. Lastly, the velocity profile for the severe case seems to strongly support the claims regarding a full reversal of the counter-clockwise vortex seen in the normal case. If it were to be compared to the velocity profile of the normal case, one would notice that it resembles a mirror image of the normal cases' velocity profile. In other words, there is a negative peak below the pulmonary valve with the highest magnitude among all of the cases, signifying that the flow is quite strong. Additionally, the remainder of the flow in the ventricle cavity exhibits an upwards flow and can be seen to be relatively stable; the velocity profile does not depict any instability, similar to the control case. This would then lead one to conclude that there is indeed a reversal of the vortex when there is sufficient regurgitation present.

The presence of a vortex reversal has been undeniably shown, quantifying this reversal might aid in the visualization and understanding of the process. In this regard, the circulation has been computed for the normal and regurgitation cases. Figure 24 illustrates the amount of circulation present in the ventricle cavity for all of the four cases. At first glance, one notices that all of the cases seem to have negative circulation, in other words clockwise circulation. This is disconcerting since all previous results point towards a counter clockwise vortex in the normal case. However, upon closer inspection, the circulation for the normal case appears to be

consistently near the zero reference line. This would imply that the amount of negative and positive circulation are of similar quantities and the resulting effect is their cancelation. This phenomenon could be attributed to the fact that the shape of the right ventricle promotes a clockwise vortex near the entrance of the tricuspid valve, ensuing in a cumulative circulation close to zero, as is seen in Figure 25. As such, one can claim that there is indeed a vortex ring present during the normal functioning of the right ventricle. In contrast, all of the regurgitation cases show clearly that they have an overall negative circulation throughout diastole, the severe case having the highest magnitude in negative circulation. This is consistent with all of the previous findings. The larger amount of negative circulation in the mild case is also in agreement with the previous speculations made. Figures 24 and 25 both show that the mild case often has a more negative circulation than the moderate case. This again could be due to the larger velocities of the regurgitant created by the small regurgitant orifice. These larger velocities aid in the formation of a more stable reversed vortex, hence explaining the larger negative circulation. A last note regarding Figure 24 is concerning the sharp drop seen in the circulation present in the regurgitation cases. Between the normalized times of 0.4 and 0.55, all three of these cases experience a sharp increase in the magnitude of negative circulation. This is most likely due to the inflow of regurgitation experienced by the ventricle and the disappearance of the vortex ring that is seen in the normal case. Furthermore, this claim is supported by the fact that the normal case does not experience any such drop, which is in consent with the actuality that there is no regurgitation present during this case.

If any more doubt still pertains to the presence of all of the structures previously discussed, a last verification was made in order to eradicate such uncertainty. The proper orthogonal decomposition was processed for all of the cases during diastole. As explained beforehand, the

proper orthogonal decomposition, in short, creates instantaneous velocity fields that represent, presumably, the most dominant flow structures present. Such velocity fields are named modes and are ranked based on the amount of kinetic energy they represent. As a standard, the first mode of every proper orthogonal decomposition is a representation of the average of all modes, hence, one might assume that the structures present in the first mode are the structures most likely present in fluid flow examined. Figure 28 shows the first two modes for all of the four cases as well as their respective average velocity fields. Although the second modes sometimes show a bit more instability, as is the case with the mild and moderate cases for instance, they show the overall trend of the fluid flow. The vortex ring no longer appears in the modes for the mild and moderate cases, suggesting that the new clockwise rotation is strong enough to overwhelm the natural fluid structures seen in the normal case. The mild case, compared to the moderate case shows a slightly less unstable clockwise vortex while the severe case seems to have the strongest and most stable reversed vortex with respect to the other cases, as can be seen from the first two modes. To further support the claim that the proper orthogonal decomposition accurately portrays the dominant structures in these cases, the cumulative fraction of modal energies was plotted, as is seen in Figure 29. If one were to reconstruct the different cases using the modes representing 98% of the total modal energy, not a lot of modes would be required. The normal case would require the least amount of modes, which is ten, indicating its modes contain a lot more kinetic energy than the other cases and that most likely the structures shown in the modes are actually present in the flow. The mild case requires slightly more modes with twenty modes necessary while the moderate case requires around twenty-three. Lastly, the severe case seems to require thirty-four modes, more than any of the other cases. The amount of modes necessary for reconstruction also speaks to the complexity of the flow. In other terms, the more

modes needed for reconstruction, the more complex the flow. This is further corroborated by the percentage of kinetic energy contained in the modes which are tabulated in Table 6. Higher amounts of kinetic energy are present in the modes for the normal case while there are less in the severe case.

After determining dominant structures developed both in the presence and absence of regurgitation, the question still remains why symptoms develop after a couple of decades after the initial operation. The answer to this question may rely in the analysis of viscous energy dissipation. Once again, the period of interest is diastole and all results presented are during that time period. The theory of the vortex reversal in the ventricle once regurgitation is present has been upheld by numerous calculations and results. There is no doubt that the counter-clockwise vortex, that is an integral part of the normal functioning of the right ventricle, changes circulation direction. However, patients with regurgitation seem to tolerate it and not require immediate surgical intervention if the regurgitation is of mild to moderate severity. This might be an indicator that it is not the reversal of the vortex itself that it causing the pulmonary valve to fail, but something else. To gain further insight, the viscous energy dissipation for all cases was computed and plotted in Figure 26. The normal case can be observed to have a fairly stable level of energy dissipation while the regurgitation cases have more eccentric plots. The moderate case is seen to have the closest plot to the normal case while the mild case has higher levels of energy dissipation. This, once again, concurs with all that has been already defended and simply speaks to the stability of the reversed vortex. However, the overall levels of viscous energy dissipation for these two cases are not terribly deviating from the normal case plot. The severe case, on the other hand, shows alarming levels of energy dissipation, far exceeding those seen in the normal case. One is then led to believe that perhaps it is the amount of dissipated energy that the right

ventricle is not able to manage. After all, the ventricle seems capable of maintaining the physical flow of the reversed vortex, implying that the ventricle is capable of adapting to changing flows. Additionally, the average amounts of viscous dissipated energy are clearly represented in Figure 27, where all of the aforementioned trends are present. Naturally, this is but a working theory and, idealistically, *in vivo* measurements would bring crucial information in order to potentially support this suggestion.

Chapter 6 - Conclusion and Future Works

Attempting to discern the flow structures present during the normal functioning of the right ventricle, let alone during the presence of regurgitation, is no simple feat. The ventricle itself is of a complex geometry, rendering the analysis of the flows seldom easy. The lack of abundant literature concerning the re-emergence of pulmonary valve failure after tetralogy of Fallot repair as well as the fluid flow in the ventricle during the presence of regurgitation adds another layer of difficulty to this research but also makes it unique since it is the first of its kind and offers novel insight into the right ventricle's workings.

The in-house cardiovascular simulator allowed for the recreation of a beating silicone right ventricle. With the use of two porcine tri-leaflet valves, the normal blood flow in the right ventricle was successfully performed while using a water-glycerol mixture that mimicked the viscosity of human blood. Once the normal flow was established, regurgitation was introduced by means of restricting the closing of the pulmonary valve's leaflets. This simulates the regurgitation that tends to appear two to three decades after the initial repair of tetralogy of Fallot. The leaflets were restricted to varying degrees in order to simulate various severities of regurgitation, thereby being able to determine any trends that could develop with increasing amounts of regurgitation.

The obtaining of the results allowed for their post-processing and their analysis. Before being able to speculate the origin of the symptoms, the normal functioning of the right ventricle and its flows must be established. The average velocity field during diastole revealed that the formation of a vortex ring is the optimal flow for a healthy right ventricle and valves. This statement was supported by several other tests such as the average velocity profile in the ventricle, circulation

and the average proper orthogonal decomposition mode. All point to this vortex being an integral part of a normally functioning right ventricle. Once regurgitation was introduced, in varying degrees, the counter-clockwise vortex was seen to reverse right away and become a clockwise vortex. With increasing regurgitation severity, aside from the moderate case, the vortex seems to stabilize in its reversed form, as seen in the average velocity of the severe case. It is hypothesized that the mild case also shows a strong vortex, compared to the moderate case, due to its small regurgitant orifice that potentially creates a stronger jet, thereby allowing the vortex to form more easily. The increase in regurgitant orifice in the moderate case could cause the two inflows to interact on a larger scale, since they are closer in size, hence creating slightly more instability than in the other cases. Once again, all of these claims are supported by results gained from the analysis of the circulation, velocity profiles and proper orthogonal decomposition.

The reversal of the vortex seemed to be accommodated by the right ventricle, speaking to its ability to adapt to changing circumstances, however, it might not be sufficient to explain the appearance of symptoms. After analysis of the viscous energy dissipation, results showed that with increasing regurgitation so do energy losses, once again the moderate case being the exception. Granted, this is likely related to the increase in backflow into the ventricle but it is hypothesized that it is these energy losses that the ventricle and valves struggle with, leading to the weakening or failure of the pulmonary valve and, if severe enough, the failure of the entire right ventricle.

Naturally, these results are only the first steps in our growing understanding of the human right ventricle and further cases must be examined in order to gain further insight into the appearance of sumptoms after the repair of tetralogy of Fallot. As such, examinations of patients and collaborations with health institution will likely aid in this endeavour. As a first follow-up

experiment, three-dimensional experimentation and analysis will exceedingly offer more information and a more complete insight into all of the structures present in a normally functioning ventricle. At which point, regurgitation can once again be introduced and the flows observed. Experiments with more variation in the regurgitation orifice might indicate the threshold at which the right ventricle can no longer adapt to the change in the flow and therefore might provide a better understanding of the optimal time for pulmonary valve replacement. Further studies emphasizing on the pressures present during these cases might also contribute to the understanding of regurgitation and potentially shed some light as to why it appears after the tetralogy of Fallot repair. And of course, observations performed *in vivo* will naturally provide accurate and actual data as to how the right ventricle copes with such changes, bearing in mind that each patient is a unique case and could provide unique insight as to how each particular heart responds to such circumstances.

References

[1] World Life Expectancy. "Canada vs USA: top 10 causes of death". [Online]. Available: http://www.worldlifeexpectancy.com/news/united-states-vs-canada-top-10-causes-of-death. [Accessed: 14- Dec- 2017]

[2] Stanfordchildrens.org."Stanford Children's Health". [Online]. Available: http://www.stanfordchildrens.org/en/topic/default?id=hypoplastic-left-heart-syndrome-90-P01798. [Accessed: 14- Dec- 2017].

[3] Tes Teach with Blendspace."Cardio Vascular System - Lessons - Tes Teach". [Online]. Available: https://www.tes.com/lessons/MZ-4a6HOs6afWQ/cardio-vascular-system, 2000. [Accessed: 05- Feb- 2019].

[4] Blausen.com. "Overview of the Cardiovascular System". [online] Available at: https://blausen.com/en/video/overview-of-the-cardiovascular-system/, n.d. [Accessed 18 Jan. 2019].

[5] Healthline. "Tricuspid Valve Function, Anatomy & Location | Body Maps". [online] Available at: https://www.healthline.com/human-body-maps/tricuspid-valve#1, 2015. [Accessed 18 Jan. 2019].

[6] Borges, N. "Tricuspid Valve Anatomy: Overview, Gross Anatomy, Microscopic Anatomy". [online] Emedicine.medscape.com. Available at: https://emedicine.medscape.com/article/1923232-overview, 2016 [Accessed 18 Jan. 2019].

[7] Waite L, Fine J. *Applied Biofluid Mechanics*. McGraw Hill, 2007, p.171-172, 165-168.

[8] Opentextbc.ca. "19.1 Heart Anatomy – Anatomy and Physiology". [online] Available at: https://opentextbc.ca/anatomyandphysiology/chapter/19-1-heart-anatomy/, n. d. [Accessed 21 Jan. 2019].

[9] O'Hara, "Mayo Clinic Radio: Structural heart disease". [Online]. Available: https://newsnetwork.mayoclinic.org/discussion/mayo-clinic-radio-structural-heart-disease/, 2019 [Accessed: 10- Jan- 2020].

[10] Mayoclinic.org. "Tetralogy of Fallot - Symptoms and causes - Mayo Clinic", [Online]. Available: https://www.mayoclinic.org/diseases-conditions/tetralogy-of-fallot/symptoms-causes/syc-20353477, n.d. [Accessed: 14- Dec- 2017].

[11] Wu J. "Tetralogy of Fallot".[Online]. Available: https://pedecho.org/library/chd/tetralogy-fallot, n. d. [Accessed: 25- Sep- 2019].

[12] Cdcgov. "Data and Statistics | Birth Defects | NCBDDD | CDC". Available at: http://www.cdc.gov/ncbddd/birthdefects/data.html, 2016. [Accessed June 27, 2016].

[13] Zaragoza-Macias E, Stout KK. Management of pulmonic regurgitation and right ventricular dysfunction in the adult with repaired tetralogy of Fallot. Current Options in Cardiovasc Med. 2013;15:575-586.

[14] Pillutla P, Shetty KD, Foster E. Mortality associated with adult congenital heart disease: trends in the US population from 1979 to 2005. Am Heart J. 2009;158:874-879.

[15] Hickey EJ, Veldtman G, Bradley TJ, Gengsakul A, Webb G, Williams WG, Manlhiot C, McCrindle BW. Functional health status in adult survivors of operative repair of tetralogy of Fallot. Am J Cardiol. 2011;109:873-880.

[16] Yoo BW, Park HK. Pulmonary stenosis and pulmonary regurgitation: both ends of the spectrum in residual hemodynamic impairment after tetralogy of Fallot repair. Korean J Pediatr. 2013;56(6):235-241.

[17] Nollert G, Fischlein T, Bouterwek S, Bohmer C, Klinner W, Reichart B. Long-term survival in patients with repair of tetralogy of Fallot: 36-year follow up of 490 survivors of the first year after surgical repair. J Am Coll Cardiol. 1997;30:374-383.

[18] Murphy JG, Gersh BJ, Mair DD, Fuster V, McGoon MD, Ilstrup DM, McGoon DC, Kirklin JW, Danielson GK. Long-term outcome in patients undergoing surgical repair of tetralogy of Fallot. N Engl J Med. 1993;329:593-599.

[19] Zomer AC, Verheugt CL, Vaartjes I, Uiterwaal CSPM, Langemeijer MM, Koolbergen DR, Hazekamp MG, Van Melle JP, Konings TC, Bellersen L, Grobbee DE, Mulder BJM. Surgery in adults with congenital heart disease. Circulation. 2011;124:2195-201.

[120] Chiu SN, Wang JK, Chen HC, Lin MT, Wu ET, Chen CA, Huang SC, Chang CI, Chen YS, Chiu IS, Chen CL, Wu MH. Long-term survival and unnatural deaths of patients with repaired tetralogy of Fallot in an Asian cohort. Circ Cardiovasc Qual Outcome. 2012;5:120-125.

[21] Shimazaki Y, Blackstone EH, Kirklin JW. The natural history of isolated congenital pulmonary valve incompetence: surgical complication. Thorac Cardiovasc Surg. 1984;32:257-259.

[22] Luijnenburg AE, Helbing WA, Moelker A, Kroft LJM, Groenink M, Roos-Hesselink JW, de Rijke YB, Hazekamp MG, Bogers AJJC, Vliegen HW, Mulder BJM. 5-year follow-up of clinical condition and ventricular function in patients after repair of tetralogy of Fallot. Int J Cardiol. 2013;169:439-444.

[23] Davlouros PA, Kilner PJ, Hornung TS, Li W, Francis JM, Moon JC, Smith GC, Tat T, Pennell DJ, Gatzoulis MA. Right ventricular function in adults with repaired tetralogy of Fallot assessed with cardiovascular magnetic resonance imaging: detrimental role of right ventricular

outflow aneurysms or akinesia and adverse right-to-left ventricular interaction. J Am Coll Cardiol 2002;40:2044–2052.

[24] Gatzoulis MA, Balaji S, Webber SA, Siu SC, Hokanson JS, Poile C, Rosenthal M, Nakazawa M, Moller JH, Gillette PC, Webb GD, Redington AN. Risk factors for arrhythmia and sudden cardiac death late after repair of tetralogy of Fallot: a multicentre study. Lancet. 2000;356:975–981.

[25] Geva T, Sandweiss BM, Gauvreau K, Lock JE, Powell AJ. Factors associated with impaired clinical status in long-term survivors of tetralogy of Fallot repair evaluated by magnetic resonance imaging. J Am Coll Cardiol 2004;43:1068–1074.

[26] Knauth AL, Gauvreau K, Powell AJ, Landzberg MJ, Walsh EP, Lock JE, Del Nido PJ, Geva T. Ventricular size and function assessed by cardiac MRI predict major adverse clinical outcomes late after tetralogy of Fallot repair. Heart 2008;94:211–216.

[27] Roos-Hesselink J, Perlroth MG, McGhie J, Spitaels S. Atrial arrhythmias in adults after repair of tetralogy of Fallot. Correlations with clinical, exercise, and echocardiographic findings. Circulation 1995;91:2214–2219.

[28] Wald RM, Redington AN, Pereira A, Provost YL, Paul NS, Oechslin EN, Silversides CK. Refining the assessment of pulmonary regurgitation in adults after tetralogy of Fallot repair: should we be measuring regurgitant fraction or regurgitant volume? Eur Heart J. 2009;30:356-361.

[29] Redington AN. Determinants and assessment of pulmonary regurgitation in tetralogy of Fallot: practice and pitfalls. Cardiol Clin 2006;24:631–639, vii.

[30] Wessel HU, Cunningham WJ, Paul MH, Bastanier CK, Muster AJ, Idriss FS. Exercise performance in tetralogy of Fallot after intracardiac repair. J Thorac Cardiovasc Surg 1980;80:582–593.

[31] Rowe SA, Zahka KG, Manolio TA, Horneffer PJ, Kidd L. Lung function and pulmonary regurgitation limit exercise capacity in postoperative tetralogy of Fallot. J Am Coll Cardiol 1991;17:461–466.

[32] Joynt MR, Yu S, Dorfman AL, Mahani MG, Agarwal PP, Lu JC. Differential impact of pulmonary regurgitation on patients with surgically repaired pulmonary stenosis versus tetralogy of Fallot. Am J Cardiol. 2016;117:289-294.

[33] Therrien J, Marx GR, Gatzoulis MA. Late problems in tetralogy of Fallot recognition, management, and prevention. Cardiol Clin 2002;20:395-404.

[34] Gatzoulis MA, Elliott JT, Guru V, Siu SC, Warsi MA, Webb GD, Williams WG, Liu P, McLaughlin PR. Right and left ventricular systolic function late after repair of tetralogy of Fallot. Am J Cardiol 2000;86:1352-1357.

[35] Valente AM, Gauvreau K, Assenza GE, Babu-Narayan SV, Evans SP, Gatzoulis M, Groenink M, Inuzuka R, Kilner PJ, Koyak Z, Landzberg MJ, Mulder B, Powell AJ, Wald R, Geva T. Rationale and design of an international multicenter registry of patients with repaired tetralogy of Fallot to define risk factors for late adverse outcomes: the INDICATOR cohort. Pediatr Cardiol 2013;34:95-104.

[36] Frigiola A, Hughes M, Turner M, Taylor A, Marek J, Giardini A, Hsia TY, Bull K. Physiologic and phenotypic characteristics of late survivors of tetralogy of Fallot repair who are free from pulmonary valve replacement. Circulation 2013;128:1861-1868.

[37] Wald RM, Altaha MA, Alvarez N, Caldarone CA, Cavallé-Garrido T, Dallaire F, Drolet C, Grewal J, Hancock Friesen CL, Human DG, Hickey E, Kayedpour C, Khairy P, Kovacs AH, Lebovic G, McCrindle BW, Nadeem SN, Patton DJ, Redington AN, Silversides CK, Tham EB, Therrien J, Warren AE, Wintersperger BJ, Vonder Muhll IF, Farkouh ME. Rationale and design of the Canadian outcomes registry late after tetralogy of Fallot repair: the CORRELATE study. Can J Cardiol 2014;30:1436-1443.

[38] Geva T. Indications and timing of pulmonary valve replacement after tetralogy of Fallot repair. Semin Thorac Cardiovasc Surg Pediatr Card Surg Annu 2006:11-22.

[39] Cincinnatichildrens.org. "Pulmonary (Valve) Stenosis in Children | Symptoms & Treatment″. [online] Available at: https://www.cincinnatichildrens.org/health/p/pvs, 2016. [Accessed 21 Jan. 2019].

[40] Mayo Clinic. "Tetralogy of Fallot - Symptoms and causes". [online] Available at: https://www.mayoclinic.org/diseases-conditions/tetralogy-of-fallot/symptoms-causes/syc-20353477, 2018. [Accessed 21 Jan. 2019].

[41] Wolfson. "Aortic valve natural remedies - The Drs. Wolfson". [online] The Drs. Wolfson. Available at: https://www.thedrswolfson.com/aortic-valve-natural-remedies/, 2017. [Accessed 21 Jan. 2019].

[42] Stanfordchildrens.org. "Pulmonary Stenosis". [online] Available at: https://www.stanfordchildrens.org/en/topic/default?id=pulmonary-stenosis-90-P01815, n. d. [Accessed 21 Jan. 2019].

[43] Shirzadfar H, Khanahmadi M. Design and Development of ECG Simulator and Microcontroller Based Displayer. Journal of Biosensors & Bioelectronics. 2018; 09(03).

[44] Mayo Clinic. "Ventricular septal defect (VSD) - Symptoms and causes". [online] Available at: https://www.mayoclinic.org/diseases-conditions/ventricular-septal-defect/symptoms-causes/syc-20353495, n.d. [Accessed 21 Jan. 2019].

[45] Ruiz M. "Overriding aorta".[Online]. Available: https://en.wikipedia.org/wiki/Overriding_aorta, 1998. [Accessed: 05- Feb- 2019].

[46] Cincinnatichildrens.org. "Tetralogy of Fallot in Children | Symptoms, Treatment & Repair". [online] Available at: https://www.cincinnatichildrens.org/health/t/tof, 2018. [Accessed 21 Jan. 2019].

[47] Surgery.ucsf.edu. "Tetralogy of Fallot". [online] Available at: https://surgery.ucsf.edu/conditions--procedures/tetralogy-of-fallot.aspx, 2018 [Accessed 21 Jan. 2019].

[48] Slideshare.net. "Adult Congenital Heart Disease - Basic Teaching Course". [online] Available at: https://www.slideshare.net/olivierfischer/compressed-tetralogy-basic-course-410131, 2013. [Accessed 21 Jan. 2019].

[49] Vitalim.ca. "Cardiovascular Diseases – Vitalim". [online] Available at: http://vitalim.ca/awareness/conditions/cardiovascular-diseases/, n.d. [Accessed 21 Jan. 2019].

[50] Healio.com. "Pulmonic valve regurgitation". [online] Available at: https://www.healio.com/cardiology/learn-the-heart/cardiology-review/topic-reviews/pulmonic-valve-regurgitation, n.d. [Accessed 21 Jan. 2019].

[51] www.heart.org. "Problem: Pulmonary Valve Regurgitation". [online] Available at: http://www.heart.org/en/health-topics/heart-valve-problems-and-disease/heart-valve-problems-and-causes/problem-pulmonary-valve-regurgitation, 2016. [Accessed 21 Jan. 2019].

[52] Mayoclinic.org. "Pulmonary valve repair and replacement". [online] Available at: https://www.mayoclinic.org/tests-procedures/pulmonary-valve-repair-pulmonary-valve-replacement/about/pac-20385090, 2018. [Accessed 21 Jan. 2019].

[53] Kheradvar A, Pedrizzetti G. *Vortex Formation in the Cardiovascular System*. New York: Springer-Verlag London, 2014, p.81-86.

[54] Hoffmann G, Lutter G, Cremer J. Durability of Bioprosthetic Cardiac Valves. Deutsches Aerzteblatt Online. 2008;105(8): 143-148.

[55] Furuse A, Mizuno A, Shindo G, Yamaguchi T, Saigusa M. Pulmonary regurgitation following total correction of tetralogy of fallot. Jpn Heart J. 1977;18(5):621-628.

[56] Pedrizzetti G, La Canna G, Alfieri O, Tonti G. The vortex—an early predictor of cardiovascular outcome? Nat Rev Cardiol. 2014;11(9):545-553.

[57] Pasipoularides A, Shu M, Shah A, Womack MS, Glower DD. Diastolic right ventricular filling vortex in normal and volume overload states. Am J Physiol-Heart C. 2003;284(4):H1064-H1072.

[58] ElBaz M, Calkoen E, Westenberg J, Lelieveldt B, Roest A, van der Geest R. Three dimensional right ventricular diastolic vortex rings: characterization and comparison with left ventricular diastolic vortex rings from 4D flow MRI. J Cardiov Magn Reson. 2014;16(1):P42.

[59] Li W, Davlouros P, Kilner P, Pennell D, Gibson D, Henein M, Gatzoulis M. Doppler-echocardiographic assessment of pulmonary regurgitation in adults with repaired tetralogy of Fallot: comparison with cardiovascular magnetic resonance imaging. Am Heart J. 2004;147(1):165-172.

[60] Grothoff M, Hoffmann J, Gutberlet M. 1064 Evaluation of postoperative pulmonary regurgitation after surgical repair of tetralogy of Fallot: comparison between Doppler-echocardiography and MR velocity mapping. J Cardiov Magn Reson. 2008;10(1):A189.

[61] Festa P, Ait-Ali L, Minichilli F, Kristo I, Deiana M, Picano E. A new simple method to estimate pulmonary regurgitation by echocardiography in operated Fallot: comparison with magnetic resonance imaging and performance test evaluation. J Am Soc Echocardiog. 2010;23(5):496-503.

[62] Falahatpisheh A, Pedrizzetti G, Kheradvar A. Three-dimensional reconstruction of cardiac flows based on multi-planar velocity fields. Exp Fluids. 2014; 55(11):1848-1863.

[63] Akins C, Travis B, Yoganathan A. Energy loss for evaluating heart valve performance. J Thorac Cardiovasc Surg. 2008;1369(4): 820-833.

[64] Shibata M, Itatani K, Hayashi T, Honda T, Kitagawa A, Miyaji K, Ono M. Flow energy loss as a predictive parameter for right ventricular deterioration caused by pulmonary regurgitation after tetralogy of fallot repair. Pediatr Cardiol. 2018;39(4):731-742.

[65] Lumley J. L. *The Structure of Inhomogeneous Turbulence*. A. M. Yaglom and V. I. Tatarski, Eds., Atmospheric Turbulence and Wave Propagation, Nauka, Moscow, 1967, pp. 166-178.

[66] Han QJ, Witschey WRT, Fang-Yen CM, Arkles JS, Barker AJ, Forfia PR, Han Y. Altered right ventricular kinetic energy work density and viscous energy dissipation in patients with pulmonary arterial hypertension: a pilot study using 4D flow MRI. PLOS ONE. 2015;10(9):e0138365.

[67] Caiazzo A, Guibert R, Vignon-Clementel I. A reduced-order modeling for efficient design study of artificial valve in enlarged ventricular outflow tracts. Comput Method Biomec. 2016;19(12):1314-1318.

[68] Guibert R, McLeod K, Caiazzo A, Mansi T, Fernandez MA, Sermesant M, Pennec X, Vignon-Clementel IE, Boudjemline Y, Gerbeau J-F. Group-wise construction of reduced models for understanding and characterization of pulmonary blood flows from medical images. Med Image Anal. 2014;18(1):63-82.

[69] Yousif MY, Holdsworth DW, Poepping TL. Deriving a blood-mimicking fluid for particle image velocimetry in Sylgard-184 vascular models. Annual International Conference of the

Institute of Electrical and Electronics Engineers Engineering in Medicine and Biology Society. 2009; 1412-1415.

[70] Eckmann D M, Bowers S, Stecker M, Cheung AT. Hematocrit, volume expander, temperature, and shear rate effects on blood viscosity. Anesth Analg. 2000; 91(3): 539-545.

[71] Jin S, Oshinski J, Giddens DP. Effects of wall motion and compliance on flow patterns in the ascending aorta. J Biomech Eng. 2003; 125(3):347-354.

[72] Nichols WW, O'Rourke MF, Vlachopoulos C. *McDonald's Blood Flow in Arteries: Theoretical, Experimental and Clinical Principles*. London, United Kingdom: CRC Press, 2011.

[73] Meschini V, de Tullio MD, Querzoli G, Verzicco R. Flow structure in healthy and pathological left ventricles with natural and prosthetic mitral valves. J Fluid Mech. 2018; 834: 271-307.

[74] Womersley JR. Method for the calcultion of velocity, rate of flow and viscous drag in arteries when the pressure gradient is known. J Physiol. 1955;127:553-563.

[75] Hart D P. The elimination of correlation errors in PIV processing. 9th International Symposium on Applications of Laser Techniques to Fluid Mechanic. 1998.

[69] Etebari A, Vlachos PP. Improvements on the accuracy of derivative estimation from DPIV velocity measurements. Exp Fluids. 2005;39:1040-1050.

[70] Stugaard M, Koriyama H, Katsuki K, Masuda K, Asanuma T, Takeda Y, Sakata Y, Itatani K, Nakatani S. Energy loss in the left ventricle obtained by vector flow mapping as a new quantitative measure of severity of aortic regurgitation: a combined experimental and clinical study. Eur Heart J-Card Img. 2015;16(7):723-730.

[71] Di Labbio G, Kadem L. Reduced-order modeling of left ventricular flow subject to aortic valve regurgitation. Phys Fluids. 2019;31(3):031901.

[72] Pearson K. On lines and planes of closest fit to systems of points in space. Lond Edinb Dubl Phil Mag. 1901;2(11):559-572.

[73] Sirovich L. Turbulence and the dynamics of coherent structures part I: coherent structures. Q Appl Math. 1987;45(3):561-571.

[74] Weiss J. A tutorial on the proper orthogonal decomposition. AIAA Aviation Forum. 2019:17–21.

[75] Aubry N, Guyonnet R, Lima R. Spatiotemporal analysis of complex signals: theory and applications. J Stat Phys. 1991;64(3/4):683-739.

[76] Fisher, Ronald (1925). *Statistical Methods for Research Workers*. Edinburgh: Oliver and Boyd. p. 47.